Experimental and FEM investigation into early gasket failure and its correlation to the clamping load and HT-PEMFC performance.

- P4 Report -

Master thesis Report

Group: HYTEC4
Dmitri Barbieru

Aalborg University
Department of Energy

Software used for simulation: Ansys Workbench, Solidworks
Software used for writing this report: Overleaf v2 Professional, Python Spyder, Microsoft Excel, Microsoft Word, Inkscape

AALBORG UNIVERSITY
STUDENT REPORT

Department of Energy
Aalborg Universitet
http://www.aau.dk

Title:
Experimental and FEM investigation into early gasket failure and its correlation to the clamping load and HT-PEMFC performance.

Project Period:
Spring semester 2023

Project Group:
HYTEC4

Participant(s):
Dmitri Barbieru

Supervisor(s):
Samuel Simon Araya (AAU)
Simon Kristensen (Blue World Technologies)
Fan Zhou (Blue World Technologies)

Copies: 1

Page Numbers: 45

Date of Completion:
June 2, 2023

Abstract:

When a fuel cell stack at is first assembled by Blue World Technology, there is a 25% chance of it not passing factory acceptance test due to various errors and performance issues. The aim of this project is to locate the source of these issues and mitigate their occurrence allowing a higher positive rate of factory acceptance tests being passed on the first try.

Summary

This master thesis focuses on high temperature PEM fuel cells than use reformate methanol. The main focus of the project was to investigate the reason behind high number of failed stacks at the infant stage of life. When the stacks are built, they must be run for at least 50 hours, sometimes even up to 100 hours before the catalyst fully activates and the fuel cell stack reaches desired performance. When individual cells in a stack show low voltage, they are repaired by changing the components resulting in time and money loss for the company.

Before the start of this project the fault was narrowed down to the gasket. But gasket is not the only component of the fuel cell and their interaction are heavily linked. To fully understand the inner workings 2 more components were investigated as a possible reason for early infant mortality rate of some cells. Leak tight tests have been performed on the bipolar plates. Bipolar plates are also leak tested after being produced meaning that they broke before or during the stack assembly. Later leak tests showed that after something critical is happening to the bipolar plates in between. The theory behind broken bipolar plates is the incorrect transportation between departments.

Even pressure distribution was of great interest as it is responsible for good sealing of reactant gases. Pressure sensitive filament has been used to analyse the pressure distribution on the membrane electrode assembly. It showed that first few cells showed unequal pressure distribution compared to the middle of the stack. It looked like the cathode and anode side are not fully sealed. Optimising the topology of the end plates and bolt positioning has been proposed as a possible solution.

Due to the fact the after changing only the gaskets during stack repair brought the cell voltage to the desired value, they received a lot of attention. They were investigated heavily under microscope for various deformations. Additional experiments have been done on new gaskets to test their limits. They were measured to determine if they were produced in the agreed upon tolerance range. The main finding from gasket tests was that they weren't manufactured with the correct shape. Discrepancies were found between technical drawings, CAD models and what was manufactured. Finite element analysis was used to show that the original gaskets, that were ordered are supposed to be 7.7% softer. Another supplier has been contacted, new gaskets were received with the correct shape. Gaskets from supplier 2 were tested to be manufactured with the right tolerances. Using them in the stacks should reduce the early infant mortality rate of cells. More tests are required to validate that statement.

Microscope analysis of gaskets has also showed an incredible amount of accumulated

dirt. The cleanliness of the work area has been put under questioning and new rules regarding clothing and cleaning standards of work area have been implemented.

Finite element analysis has also been used to propose different designs for the gaskets that combine the soft aspect and improves on the gasket slippage. The new proposed designs have also optimised the stress distribution across the lips of the gasket moving the stress concentrations from weak points. Finite element analysis was also critical in providing more insight into gasket behaviour such as the deformation and slippage.

From experimental work gasket and membrane electrode assembly stiffness were calculated. The results were used to find an optimal clamping load for a stack. Clamping load influences the porosity of the gas diffusion layer, mass transport and contact resistance. By default the stacks are build using 19,620 N force. New clamping load of 13,734 N was proposed. A new stack has been built and tested in the range of 9,810-24,525 N. The experiment showed that the voltage kept increasing with the clamping load past the usually used one. Two outcomes are possible from these findings: keep increasing the clamping load until the voltage starts to decrease and test the influence of different clamping loads on the degradation rate of the stack. It is a concern that the 19,620 N clamping force is over compressing the gaskets and membrane electrode assemblies resulting in lower life expectancy.

Preface

This Master thesis was written by Dmitri Barbieru (Dima) as a collaboration project with the company Blue World Technologies located in the city of Aalborg, Denmark. The topic was investigating the reason behind low first pass yield of fuel cell stacks. Gaskets were identified as the main culprit behind low voltage performance, so they became the main focus of investigation.

But gaskets are not the only component in a fuel stack, bipolar plates and membrane electrode assembly components have also been touched upon. Research has been performed into the topics of usual assembly errors of fuel cell stacks, research that inspired to perform experiments with prescale fuji film, microscope imaging of components, optimising the clamping load and finite element analysis.

I would like to thank my supervisors Simon Kristensen, Fan Zhou and Samuel Simon Araya for the support and guidance during the process of my thesis. I would also like to give the shout out to Mads Bang for asking some very good questions and his guidance during the FEA stage of the project. This thesis wouldn't be complete without intensive knowledge shared on creation of bipolar plates and membrane electrode assemblies by the chemical team: Denys Gromadskyi and Larysa Hromadska. Furthermore, I would like to thank my almost wife and friends for emotional support during the tough times.

Nomenclature

Acronyms	Description
FC	Fuel Cell
PEMFC	Proton Exchange Membrane Fuel Cell
HT-PEMFC	High Temperature Proton Exchange Membrane Fuel Cell
STP	Standard Temperature and Pressure
MEA	Membrane Electrode Assembly
MEM	Membrane
BPP	Bipolar Plate
FAT	Factory acceptance test
GDL	Gass diffusion layer
CVM	Cell voltage monitor
COR	Contact ohmic resistance
EP	End plate
FEM	Finite element method
FEA	Finite element analysis
PTFE	Polytetrafluoroethylene
PPS	Polyphenylene sulfide
N	Newton
V	Voltage

Contents

List of Figures

List of Tables

Chapter 1

Introduction

As of 2023 there are 1.44 billion vehicles in the world. Most of them running on either gasoline or diesel [1] and the share of newly produced cars in Q3 2020 consists of only 11% battery cars, 22% hybrids while the rest are still running on either gasoline or diesel in EU. A union of countries that are already focusing on greener transportation [2]. While it is a step in the right direction to mitigate the climate change it can be argued to be a minuscule step and taking it too slow. Some argue more drastic automatisation is needed with bigger funding for preventing the impeding disasters caused by climate change.

When adding the maritime industry into the equation, the largest 16 ships emit the same amount of CO2 as all the world's cars combined together [3]. Taking into consideration that the whole transportation industry is responsible for a total of 16.2% global CO_2 production [4], it's no surprise that a lot of companies are trying to decarbonise this sector by either producing more electrical vehicles or integrating hydrogen fuel cells into trains, busses, cars and ships [5].

In order to achieve this goal, it requires an accelerated production of fuel cells, automated to the highest standards of automobile and maritime industry. The lifespan of fuel cells must be equal or surpassing that of classic combustion engines. Hyundai for example set a goal to fully automate their hydrogen combustion engines by 2025 [6] While it is not exactly a fuel cell, it does illustrates the importance of automation for mass market of hydrogen solutions to be widely and cheaply available if humanity is to save the current ecosystem of this planet we call our home.

While the degradation and lifespan of a fuel cell is an important topic, this thesis will focus on the quality of assembly and factory acceptance tests. This thesis will analyse the reason behind some stack's failure rate at infant mortality stage and will propose and test hypothesis to increase the number of freshly build stacks that pass the factory acceptance test on their first attempt.

1.1 Problem Statement

75% stacks built by the company pass their factory acceptance tests. It is considered a low number. Investigation is done with focus on stacks failure at the beginning of life period.

1.2 Fuel Cell

Fuel cell stack consists of multiple cells that are stacked together. One single cell is an assembly of the following components as illustrated in the figure 1.2: Membrane electrode assembly (MEA) that is an assembly of a few components responsible for the

	90 cell	160 cell
Production W38 & W39	5	7
Passed	2	6
Failed	3	1
PFY	40%	86%
FPY combined	**72,6%**	

Figure 1.1: First pass yield of 72,6% calculated by the production in week 38 and 39.

electrochemical reaction such as gas diffusion layer (GDL) that is coated with precious metals to facilitate electrochemical process. The membrane (PEM) isolates reactant gases and transports protons by using acid. Gasket provides sealing of reactant gases and prevents any leaks and crossover. Bipolar plate (BPP) transports reactant gases and coolant.

To build a stack multiple cells and a few more components are required: end plates (EP) with bolts that will clamp the whole structure together and current collector plate in contact with the bottom end plate and the adjacent cell to close the electrical loop and assist in a better electrical transfer. Some stacks also have an insulation plate between end plate and current collector to isolate the end plates.

The stacks and their components were provided by the company and their specific material composition will not be stated in this paper.

Fuel cell stacks build at the company have a 75% first pass yield rate during factory acceptance test (FAT). Figure 1.1 shows 72.6% in week 38 and 39 which is even worse. FAT is not passed when cell voltage monitor (CVM) shows a low voltage. CVMs show which cells are not at their ideal performance and helps point to the exact cells that are in need of repair by replacing failed components with new ones.

Low pass yield results in time wasted on the repair of stacks by finding the correct cells that need to be changed and repaired. Considering that some stacks can have as many as 160 cells or even more, it does waste a lot of precious time from personnel to focus on this problem. Multiple things can go wrong during the assembly process, any part of a cell could be critically damaged or manufactured with low tolerances. It also makes it necessary to order new expensive components to change the faulty ones, further resulting in money loss.

To narrow down the faults, various experimental work has been performed on the following components to determine which ones have a higher chance of failure and the reason of the failure, while trying to provide a solution and a mitigation strategy for improving the reliability of the assembly and increasing the FAT acceptance rate.

1.2.1 Bipolar plate (BPP)

The BPP collects current generated by the electrochemical reaction, distributes fuel, oxidant and coolant. It is manufactured out of 2 monopolar plates that are glued together.

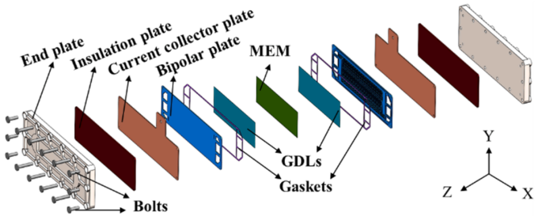

(a) Exploded view of 1 cell stack assembly shows the order of assembly and design of a rectangular shaped cell consisting of membrane (MEM), gas diffusion layer (GDL), bipolar plates (BPP), gasket, end plates (EP), collector plate, insulator plate and bolts [7].

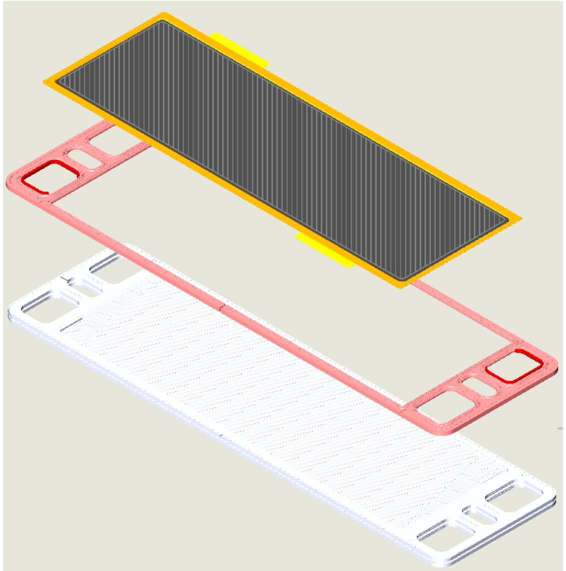

(b) Exploded view of 1 cell: Bipolar plate, gasket and MEA.

Figure 1.2: Exploded view of 1 cell assembly.

Each side is responsible for the transport of either oxygen or hydrogen rich gas, while the middle cavity acts as coolant channel.

BPP can be manufactured either out of metals or carbon black compound, first ones requiring welding monopolar plates together, the second ones require gluing. Both materials have their advantages and disadvantages. Carbon black for example is less dense but also less resistant to stresses. BPP used in this report were made out of carbon black and Polyphenylene sulfide (PPS). Properties and behaviour of BPPs under stress were studied.

Some of the required properties of BPP are good electrical conductivity with as little resistance as possible, hydrophobic properties preventing the gas crossover and giving it a low flow resistance. Hydrophobicity of the BPP is also important so that it doesn't absorb any acid into its structure. Low density and porosity ratio and good structural strength [8] are also critical aspects. All of this the author had to keep in mind when working with them. For example, when structural integrity of the BPP is lowered, internal cracks occur preventing them being leak tight which will be seen in the following chapters.

As the theme of this thesis are assembly problems and early failure rates, common BPP problems were researched. Some of the most common errors of BPP can be attributed to the gluing process or low tolerances illustrated in figure 1.3a. It can result in gas crossover between the anode and cathode side, and sometimes even in oil leak either into the anode or cathode side ruining the MEA. Assembly error are another cause of

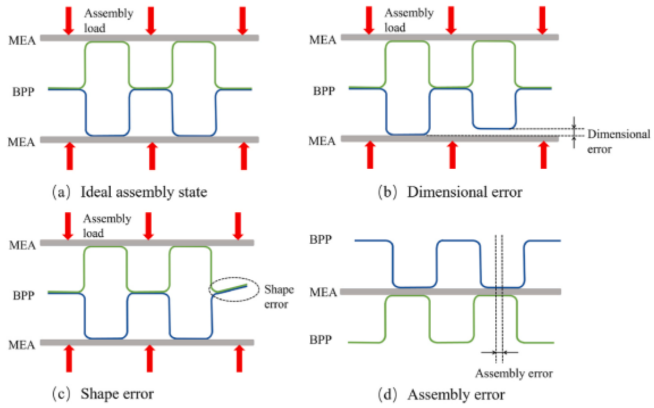

(a) Error types of BPP: (a) ideal assembly state, (b) dimensional error, (c) shape error, (d) assembly error [9].

(b) Plastic deformation left on GDL surface due to compression of BPP channels into the MEA [10].

Figure 1.3: Assembly error of BPP and plastic deformation on the GDL surface.

BPP failure as handling and transporting can damage them, some cracks can be invisible to the human eye without use of X-ray and microscope.

1.2.2 MEA

As mentioned above, MEA is an assembly of 2 GDLs and a (PEM) membrane with a catalyst layer on GDL. It is responsible for the electrochemical reaction and produces electricity in the fuel cell. PEM is very thin and very papery giving it low structural strength with high flexibility. The GDL is a conductive porous material coated with Polytetrafluoroethylene (PTFE). PTFE exhibits hydrophobicity, a necessary quality for a chemical that might be banned soon by the European Union [11]. The hydrophobicity of the GDL makes sure that it never gets clogged with water, as it will reduce the gas transport to the catalyst layer (CL). A lot of future research will have to focus on changing the chemical recipe for the MEA. The acid in the GDL is also critical for proton transportation [12]. Besides that, GDL also provides mechanical support for the CL. In general the porosity and permeability of the GDL affect the rate of electrochemical reaction influencing the performance of any PEMFC [13].

Over compressing the MEA with an excessive clamping load will force the BPP channels into the GDL creating a large shear force that might cause damage to the GDL fibers. Excessive clamping load will also squeeze the GDL fibres reducing its porosity, reducing the mass transfer of reactant gasses. After disassembling the stack, marks from BPP can be clearly seen on the GDL layer due to plastic deformation as shown in figure 1.3b which appears to be a common occurrence in PEMFC. Reference [14] comments that clamping load should be designed as small as possible as long as contact ohmic resistance (COR) between GDLs and BPPs is as low as possible and the stack is leak tight.

Due to tolerances in production of BPPs the rib length and channel height can vary

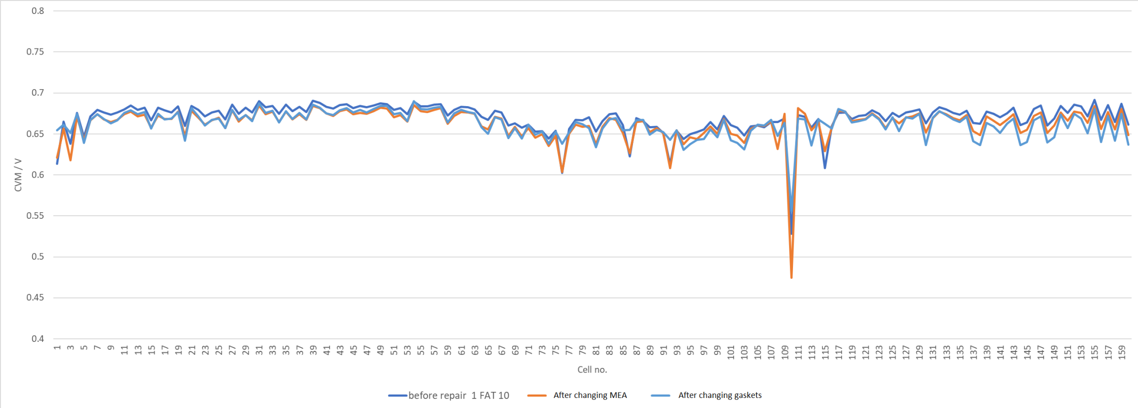

Figure 1.4: CVM performance before and after changing gasket.

and not be of exact dimension. These variations are also the cause of uneven clamping load distribution on the GDL resulting in uneven distribution of current density and uneven heating which might cause hot spots in the MEA and subsequently accelerating the degradation[9].

Besides creating an uneven temperature distribution, it also results in reduced mass transfer, that also affects the overall performance of the PEMFC stack.

The clamping load distribution thus is of great interest in this thesis and was analysed from a few key points. Therefore, it was important to find the minimum clamping load for stack at which it could be leak tight and stable. Then going from there to see how do different components and the stack itself behave under different clamping loads to nail down a more optimal value. An important note about MEAs used in all tests, is that their ideal compression should be of only 0.1mm which was found from previous experimental work done by the company. This 0.1mm compression will be further used in this report in the following chapters.

1.2.3 Gasket

Gasket provides sealing between adjacent BPPs preventing leakage of fuel and oxidant. It must withstand operation at higher temperatures without degrading. Ref [8] mentions that improper designs can cause sealing failure during assembly and operation of larger PEMFC stacks.

Due to the design of the BPP, the gasket used in this report can't be compressed by more than 0.45mm or a 24.3% compression. The ideal gasket compression supplied by the manufacturer is in the range of 15% to 30%. Knowing tolerances from manufacturer regarding the gaskets, the compression value of gaskets can be between 21.9% and 27.3%. Considering that most of the deviations are within the acceptable limit of the gasket material property, the ideal compression of 0.45mm will be mostly used to determine the expected stresses and deformations of the gasket.

The gaskets analysed in this report appear to be the main culprit behind a lot of failed

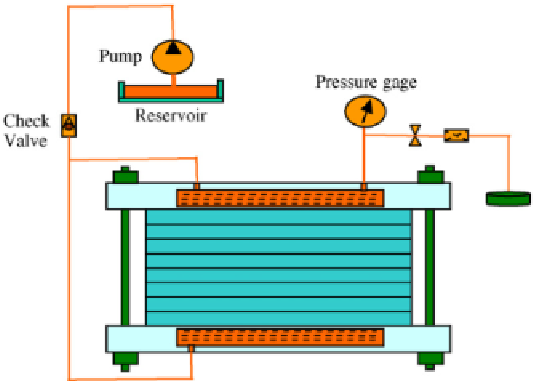

(a) Schematic of compression system design of EP [15].

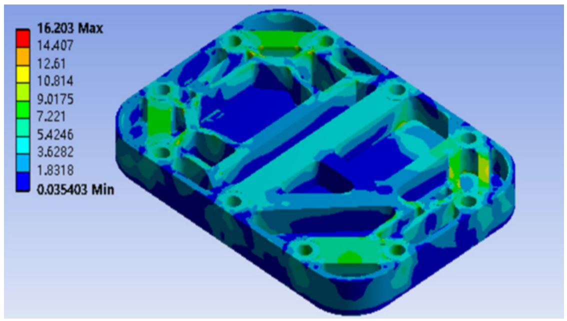

(b) Stress distribution of topology optimised EP using FEM analysis [16].

Figure 1.5: Different solutions for improving clamping load distribution of the end plate.

cells in various stacks illustrated in figure 1.4. Figure shows the voltage of each individual cell of the repaired stack. After the second repair when the gaskets have been changed, cells 75 87, 115 and a few others have seen their voltage improving. The main conclusion was that changing only the gasket during the repair brings back the CVM to the acceptable performance. Consequently, many experiments and analyses have been focused on gaskets themselves with the constant question: why are gaskets responsible for stack failure? Aspects such as: gasket compression, gasket design and FEM analysis of different gasket designs to improve the sealing have been researched.

1.2.4 End plate

Endplates fastened by bolts provide clamping load on the stack. EP requirements are: sufficient strength, small volume, light weight and easy processing [9]. The most common design consideration of EP is its ability to not deflect. Active hydraulics endplates have been proposed by some to prevent deflection using thinner EP to reduce weight[15] while other researchers have focused on optimising the stress distribution by optimising the design of the EP and the bore holes placement for bolts using different pretension values [16] [7].

Compared to building an active hydraulics system, changing the design of the EP seems a simpler and cheaper option. It does require FEM analysis though on the current operating EP with topology optimisation. Unfortunately, during this thesis there wasn't enough time to investigate the optimisation of EP. Although the author agrees that having deeper insight into EP design is required to achieve a better clamping load distribution on the cells in a stack. As it stands, only experimental work using prescale fuji film was used to analyse the load distribution together with FEM analysis on gaskets.

1.3 Quality issues

Sections above discuss some potential failure modes for specific parts of a stack. This section is a summary of some quality issues that were observed during the research done for this paper that can't be attributed to just one component. While some of the following issues have been addressed and fixed, others are still being investigated in more details:

1. Measurement accuracy in some test set-ups are questionable. It results in spending a lot of time in setting up an experiment, waiting for results and validating those results. Some of the experiments in this paper had to be repeated 3 or more times before trustworthy results could be achieved. An example of that would be measuring the compression of 21 gaskets that is described in Chapter 4. First time, unstable hydraulic press was used that couldn't hold the clamping load stable. By the time the author started measuring the height of the stack from the back side it would lose 981N of pressure. Some measurements were wrong when the author forgot to re-apply the pressure every 1 minute. Next time, a more stable hydraulic press was used, with an old design of end plates usually used in tests. The old design of the EP that caused disproportional bending in the middle until a released version of the EP was used.
2. Bad factory layout causes too much movement of fragile components between buildings. Simple example is moving BPPs using a table with hard wheels over an uneven road filled with potholes. It creates a lot of vibrations when transporting, naturally resulting in some bipolar plates to developing micro cracks during the transportation after which they couldn't pass a second leak test.
3. Low standards of cleanliness in the production area. Lots of dust and some human hairs have been found in cell components during postmortem.
4. Human error results in some quality issues during the assembly. More training time focusing on quality is required.

Chapter 2

Experimental Methods

The main problem and challenge of this thesis is that stacks fail at the start of life after assembly. It requires repairs to bring them to required performance. This chapter breaks down all the experiments and the reason behind them with intention to find the fault behind high failure rate of stacks. The results from these experiments are presented in the next chapters.

2.1 Compression force distribution measurements

Prescale Fuji film also known as pressure sensitive film is a paper filled with ink trapped in small bubbles. When a pressure is applied to the film, the bubbles rupture and release the ink. The ink colours the paper with a red paint. The higher the pressure is applied to this film, more bubbles rupture that releases more ink. Subsequently colouring the paper with a higher intensity of red shade, giving the user an idea of how the pressure is distributed. Figure 2.1b shows how to read the colour intensity depending on the prescale film selected, relative humidity and temperature in the room. There is a wide range of Fuji film that can be ordered and they are divided by the range of pressure they are subjected to from 0 to 300 MPa [17].

$$P = F/A \tag{2.1}$$

To find the correct prescale film equation from above was used. Where P is the clamping pressure, F is the clamping force and A the surface area of the cell. The surface area of the cell is given from design and force decided to be in the range of 9806-29,430 N. Clamping pressure was calculated to be close to 0.5 MPa and the corresponding pressure sensitive film (LLW) was ordered.

Prescale film comes in two types, two sheet type and mono type. Prescale film of required pressure range came as two sheet type, as illustrated in figure 2.1a. Both films have to be cut to the exact same size 403mm x 113mm to cover the BPP then placed on top of each other as shown in the instruction's manual.

The stack should be built as it is usually done. The prescale film with 2 GDLs should be inserted instead of MEA as shown in figure 2.3 and 2.2. 1 Prescale film and 2 GDLs are of the same thickness as 1 MEA. The prescale film shall be placed on top of 2 GDLs.

After the stack is built with prescale film instead of membrane, clamping force is applied. Clamping force should be held for 2 minutes to simulate the continuous operation then released. The prescale film should be safely and accurately taken out without damaging it as it is sensitive to the slightest pressure even such as human thumb touches as can be seen in some pictures in the following chapter. The experiment was repeated under the following clamping loads:

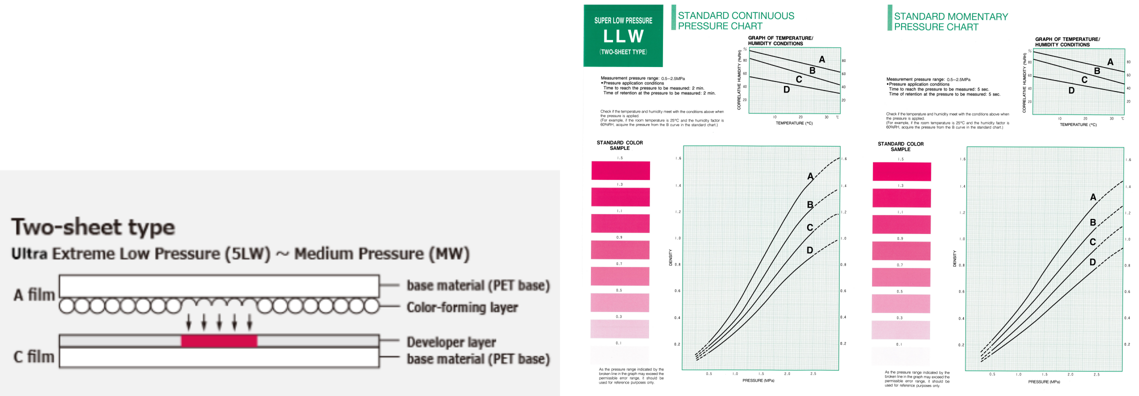

(a) Two sheet type of prescale film. Film A contains colour forming capsules that break when pressure is applied. Film C has developing layer, that absorbs the liquid and changes the colour to red [17].

(b) Pressure chart of LLW prescale film. Left side shows results for simulation of long exposure to a load, left side shows results for simulation of an impact to the desired object [17].

Figure 2.1: Prescale instruction manual.

- 1,500 kg & 0.38 MPa
- 1,750 kg & 0.45 MPa
- 2,000 kg & 0.51 MPa
- 2,250 kg & 0.57 MPa
- 2,500 kg & 0.64 MPa

The bulk electrical resistance and interfacial contact ohmic resistance (COR) are strongly influenced by the clamping load applied to FCs. Increasing the compression under low current density increases the output power of the FC while at higher current densities the output power decreases due to reduced porosity of the GDL, as its being compressed too tight and increases flow resistance for oxygen transport [19]. Most of the researchers agree that there is an optimal clamping pressure on a FC stack. Too low clamping will result in bad sealing and too high pressure will reduce the porosity of the GDL increasing the resistance too much, with a risk of breaking the BPP. Optimal clamping load can be found through experiments discussed in next sections.

Looking at clamping load distribution over MEA will also give an insight if the load is evenly distributed across the whole BPP and MEA. It also gave an insight into gasket, as it was interesting to find if it seals all edges of BPP with an even force. Most papers agree that clamping force results in an even pressure distribution in the middle of the stack. Even so, the first few times prescale film was testes on a 5 cell stack before looking at a 160 cell stack due to the limit of available stacks for this test.

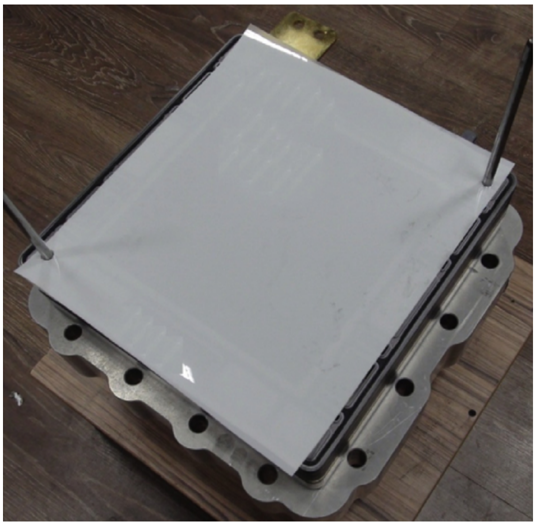

Figure 2.2: Position of prescale film on the BPP should cover the BPP and gaskets allowing to see the pressure distribution on both the sealing gasket, MEA and BPP [18].

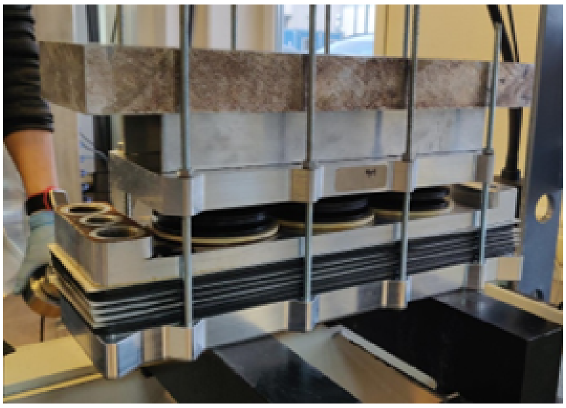

(a) Measuring the compression force distribution in a 5 cell stack between each BPP.

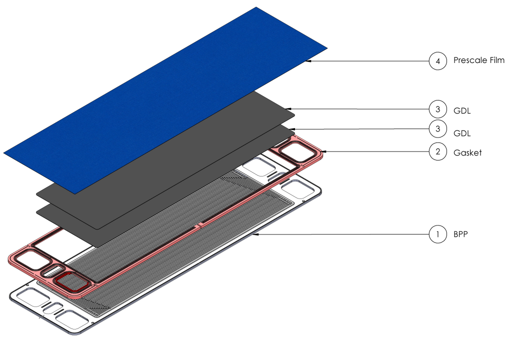

(b) Illustration of correct assembly of one cell where the prescale film is placed instead of membrane.

Figure 2.3: (Left) stack build with prescale film. (Right) assembly instructions for building a cell with prescale film.

2.2 BPP

Bipolar plate is also a very important structure in a PEM FC stack, sometimes exceeding 60% of weight of the stack and 30% of manufacturing cost [20]. As it makes the bulk volume of the stack it must have very good mechanical properties to increase the durability, low electrical resistance as it transports electrons. It has to be low density to decrease the weight of the stack finding the right spot between density and porosity which would reduce the structural strength. It also transports coolant and reactant gases through its channels, so it is critical that all channels have low flow resistance.

2.2.1 Leak test

In some cases when a FC stack shows low cell voltage it can be due to leaks from individual cells. They can be easily found when a stack is built, but there could be multiple reasons why the any individual cell is leaking. This section will explain the experimental method used to find out which BPP were manufactured under low tolerance and couldn't properly seal gases inside.

One of the stacks showed extremely bad performance, and multiple leaks were detected when pressure tested. It was taken apart and each individual BPP was tested. For the test set up a hydraulic press was used to clamp a 1 cell stack. 1 cell stack consisted of 2 end plates, gasket, GDLs and a single BPP. No MEAs were used during this experiment. The BPP was clamped with a clamping force of 4,905 N, then pressurised to 1.50bar at the anode, cathode and coolant side. The pressure was recorded and compared after 3 minutes. If the pressure dropped by more than 0.01bar the plate was failed.

Second stage was to drop the pressure on the coolant side to 1.20bar while keeping the cathode and anode pressure at 1.50bar. The pressures were noted and compared after another 3 minutes have passed. 0.3bar difference was chosen because having a bigger pressure difference might damage the MEA. 0.3bar is the safe option that reveals if the BPP is not leak tight, at the same time not damaging any other components. During this stage cross flow between anode and cathode to the coolant side is a point of interest, as potential bad BPP could allow hydrogen and oxygen gases to flow into the coolant side due to the 0.3bar difference in pressure between the channels. A pressure drop in anode and cathode and coolant pressure increase of 0.01bar resulted in failing the BPP as not leak tight.

2.3 Gasket

Gasket is the main sealing agent in a cell and its material composition need to be able to withstand harsh environments as it works under high temperatures around 160°. Gasket is in contact with graphite and MEA containing phosphorous acid under relatively high clamping load. Clamping load that must also create a good enough seal to prevent any fuel, oxide or coolant leaks [21] [22].

During FAT some cells of multiple stacks showed reduced performance. While attempting to find the fault and repair the cells, it was found that changing only the gasket in the faulty cells improved the voltage to the desired output. To investigate this phenomenon further several experiments have been performed to analyse possible causes of the gasket failure and its influence on stack performance.

Before the first experiment, several groups of gaskets were defined as good, bad and new gaskets:

1. good gaskets: gaskets removed from cells showing good performance.
2. bad gaskets: gaskets removed from cells showing below desired voltage.
3. new gaskets: gaskets that have not been used before.

2.3.1 Compressibility and elasticity

Gasket at rest was measured across the perimeter at 8 points shown in figure 2.4a. Normal 7 cell stack was assembled and the height of the stack was measured across the same points shown in figure 2.4b and 2.5. Knowing the thickness of the bipolar plates (BPP) and end plates (EP) its possible to find the exact distance of compression for the gaskets. The stack was compressed to the following pressure then remeasured across the same points for each compression step. The compression is with a step increment of 2,453 N starting at 2,453 N until 4,525 N.

After the first attempt, to further improve the accuracy of this test, another set up was used with a new step increment of 981 N, starting from 0 N until 24,525 N. Two 20 cell stacks were built. One stack was built out of: BPPs, gaskets, released end plates. The second stack was build using: BPPs, MEAs and released end plates. All in order to calculate the compression stiffness of both the gasket and the MEA.

Gasket thickness was measured before compression to compare with technical specification and check the tolerances. Specific quality control design verification test was written and implemented that exists only to check the gasket dimensions before they are used in building a stack.

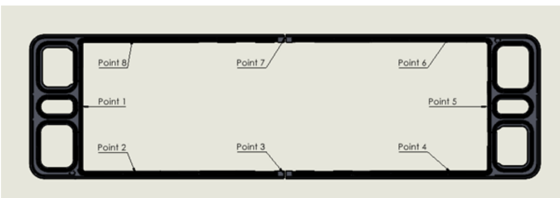

(a) Points of interest in a gasket that were measured to determine the total thickness.

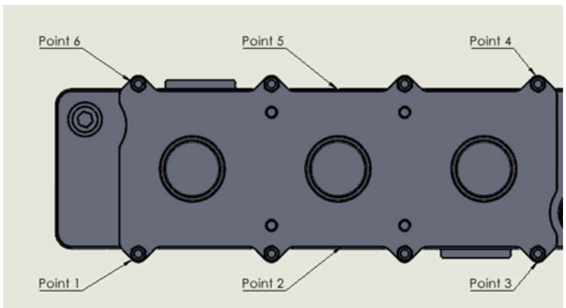

(b) Points of interest in an assembled stack that were measured to determine the compression of a stack. View from above.

Figure 2.4: Measuring points on the gasket (left) and the stack(right).

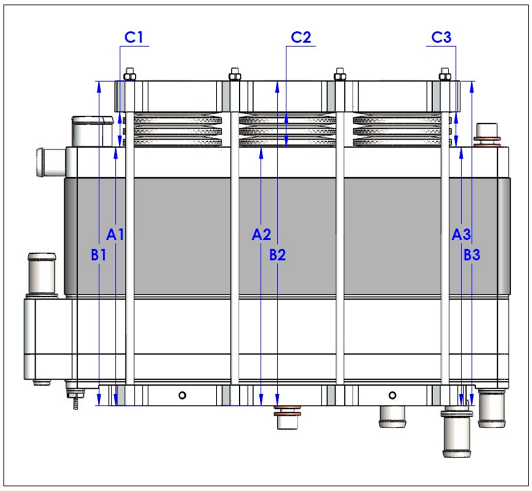

Figure 2.5: Measuring points of stack height.

2.3.2 Microscope imaging

Microscope imaging was used to detect topographical changes on the gasket surface. At first it was performed on 1 new gasket to note its lack of defects, then 3 good gaskets to know which defects might be acceptable and 3 bad gaskets. Photos were saved on the PC in the highest resolution possible of 4k then send to all interested parties.

After the first round of microscope imaging the experiment was repeated on new gaskets that have been compressed to different clamping pressures to find a correlation between number of cuts and clamping load used to assemble a stack. It was of interest to find out if the clamping load was exceeding the maximum allowable stresses and stretching the gaskets beyond the elastic deformation limit. FEM analysis has been performed to validate those findings.

The gaskets in the second experiment were compressed with a step increment of 2,453 N starting at 4,905 N until 24,525 N clamping force was achieved. The gaskets were marked and kept separately from each other to avoid confusion. Each individual gasket has been thoroughly analysed from all sides.

2.4 Finite element method

Finite element method has been used to analyse and get more insight into the behaviour of the gaskets during the stack assembly such as gasket deformation, stiffness and Von-Misses stress.

Von-Misses stress has a scalar quantity that is obtained from all stresses acting on any structure independent if its symmetrical or not. It predicts the yielding stress of materials under complex loading [23]. It helps engineers find out if the created stresses will reach the yielding point or not.

Material Model	Recommended Strain Range
Neo-Hookean	<30%
Mooney-Rivlin	<200%
Arruda-Boyce	<300%
Polynominal	<300%
Ogden	<700%

Figure 2.6: Ansys material models [24].

Due to nonlinear behaviour of the gasket, nonlinear method has been applied with large deflections. To gain more accurate results the material properties have been fitted to experimental data. The experimental data and material properties of hyper elastic materials from Ansys's database followed the same trend that had to be slightly adjusted [24].

Hyperelasticity: There is no constant factor like Young's modulus in metals to relate stress to strain. Hence the relationship is derived from strain energy density function [24] and governed by the following equation:

$$S_{ij} = \frac{\partial W}{\partial E_{ij}} = 2\frac{\partial W}{\partial C_{ij}} \tag{2.2}$$

S_{ij}= components of the second Piola-Kirchhoff stress tensor

W= strain energy function per unit undeformed volume

E_{ij}= components of the Lagrangian strain tensor

C_{ij}= components of the right Cauchy-Green deformation tensor

Figure 2.6 shows material models that use energy density function with a recommended strain range. The strain range for the gasket while being closer to 30%, using Neo-Hookean didn't provide satisfactory results, while Mooney-Rivlin 5 parameters [25] could get very close to the real data making fitting the material properties easier to accomplish.

The end goal of the FEM analysis is to optimise the gasket topology by analysing the total deformation under 0.45mm compression, Von-Misses stress [23] and Force reaction on y-axis created by the compression giving results for gasket stiffness.

Simple 2D BPP and gasket were redrawn in Solidworks and imported to Ansys Workbench. Material properties for BPP were taken from production. While gasket properties had to be found out through experimental work than fitted into the model.

Top BPP was displaced 0.45mm on y axis. Bottom BPP was constrained as fixed support. All possible contacts were set to frictional with 0.3 coefficient. Mesh was nonlinear with squares and triangles combined. The simplified 2D geometry didn't require pure triangles. The edges were refined where necessary.

Large deflection was used, with iterative step convergence. Non symmetrical Newton Raphson was used to help the convergence. Due to high deformation, adaptive mesh was introduced to help with re-meshing when necessary. Iterative and Newton Raphson methods are used for nonlinear problems. When deformation equation equilibrium can't be reached on the first try, they are used. They calculate deformation with each step using the results from previous step until energy balance is reached [26].

Chapter 3

Bipolar plates and MEA

As described in previous chapters MEA is an assembly of a few components. Depending on the quality of the assembly the MEA can be ruined even before inserted into the stack. Distribution of the clamping force quickly becoming the focus point of this project, the clamping load distributing was investigated over the MEA. The first part of this chapter focuses on those results.

The second part of this chapter shortly evaluates the findings of leak testing the BPP. Bipolar plates are created out of a slurry of graphite and mixing agents with fluoride to give it hydrophobic properties. It is then dried then pressed into monopolar plates that are glued into bipolar plates. If not aligned perfectly the gluing process can create deformations inside the BPP. Likewise, due to the material being brittle when subjected to sudden forces it might crack losing its sealing properties.

3.1 Compression forces distribution

First use of prescale film was on one 7 cell stack. The prescale film was placed on the top cell instead of MEA as instructed in figure 2.3b on top of the 2 GDLs. Four clamping loads were used as shown in figure 3.1. Skipping the force of 19,620 N as it's the normal assembly force and is measured in the next experiment.

First experiment shows 2 round spots with higher compression, and 1 spot in the middle with lower load distribution. It can be attributed to the usage of the end plates used for testing the performance of the stacks. Changing EP to a new released version of EP shows an improvement in the load distribution.

Figure 3.2 and 3.3 show the result of the second and third attempt at this experiment. This time 1 steady load was used, 19,620 N and a 5 cell stack was built instead of 7 cells. The observable differences in second and third experiment can be attributed to user error from using 4 GDLs instead of 2 GDLs, which gives a softer outline as a lot of compression forces were absorbed by the extra amount of GDLs instead of being transferred to the BPP and gaskets.

During the second test 2 different sets of gaskets have been used. The scanned papers have been noted with the type of gasket used. Gaskets from cells with bad performance and gaskets from cells with good performance. It was interesting to find out if it's possible to see any difference in load distribution between the good and the bad gaskets.

Figure 3.3 shows the final result of the prescale film test. A gradual decrease in even load distribution can be seen going from the bottom to the top, from the first to the fifth cell. First cell being on the bottom and fifth cell being on the top. Usually [18] the load distribution is worse on the first 5 top and 5 bottom cells. It is supposed to improve when moving into the middle of the stack which can be seen in figure 3.4. Big stacks have an

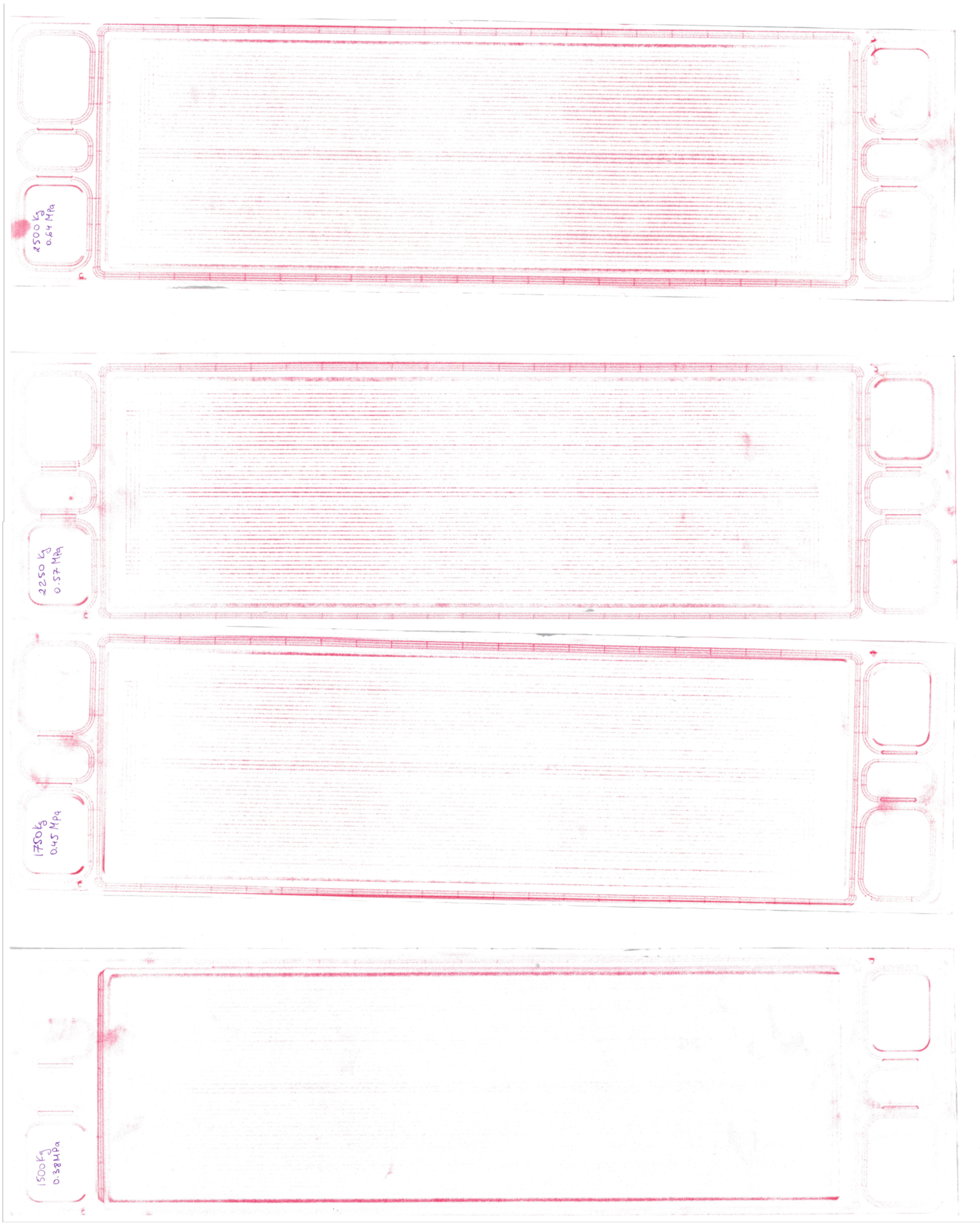

Figure 3.1: First test using prescale film to see pressure distribution on stack under different clamping load. Using new gaskets.

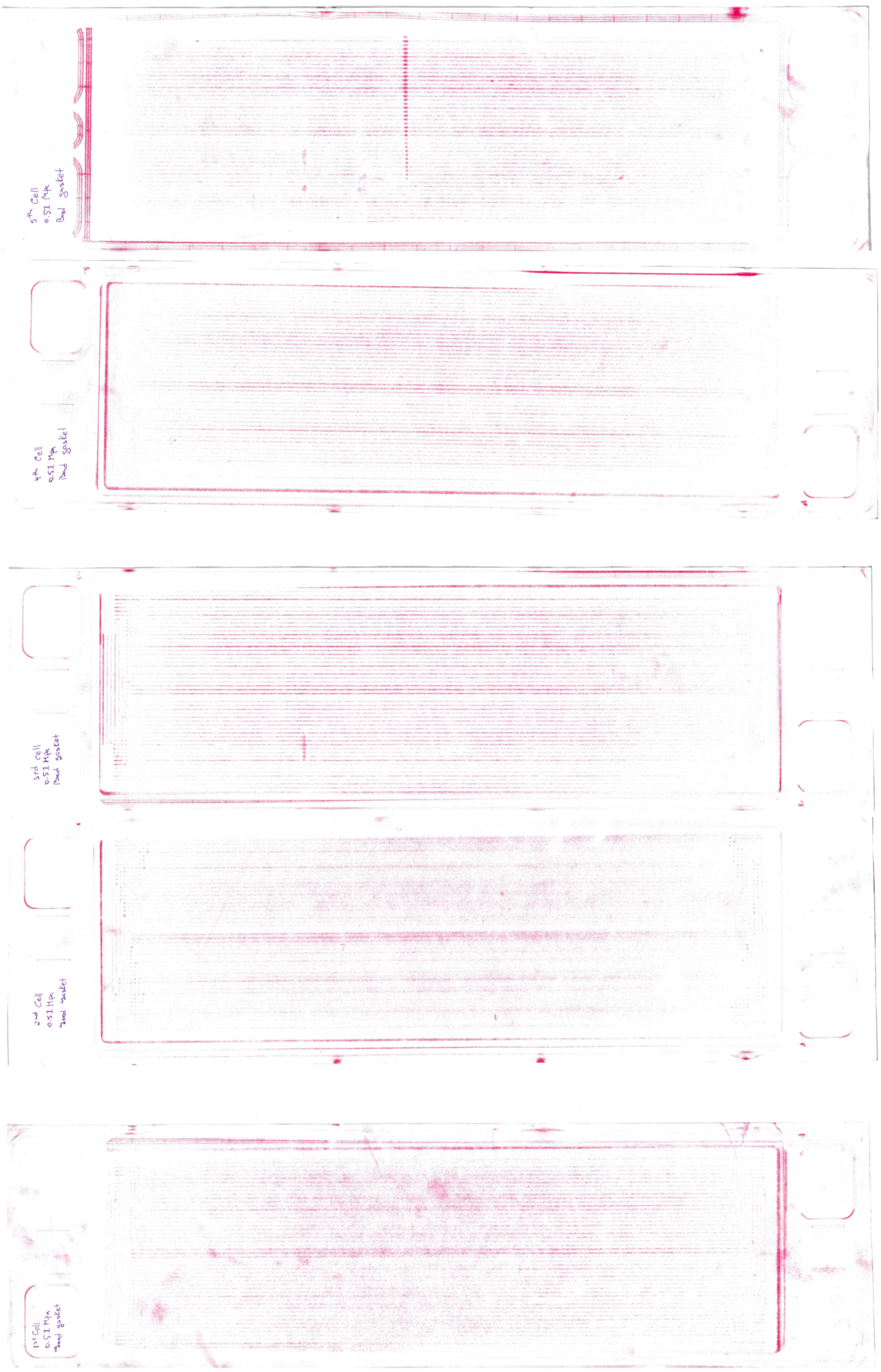

Figure 3.2: Second test using prescale film. Stack of 5 cells has been built. All cells were measured at the same time at clamping force of 19,620 N. 4 GDLs have been used. 2 batches of gaskets have been used, good and bad.

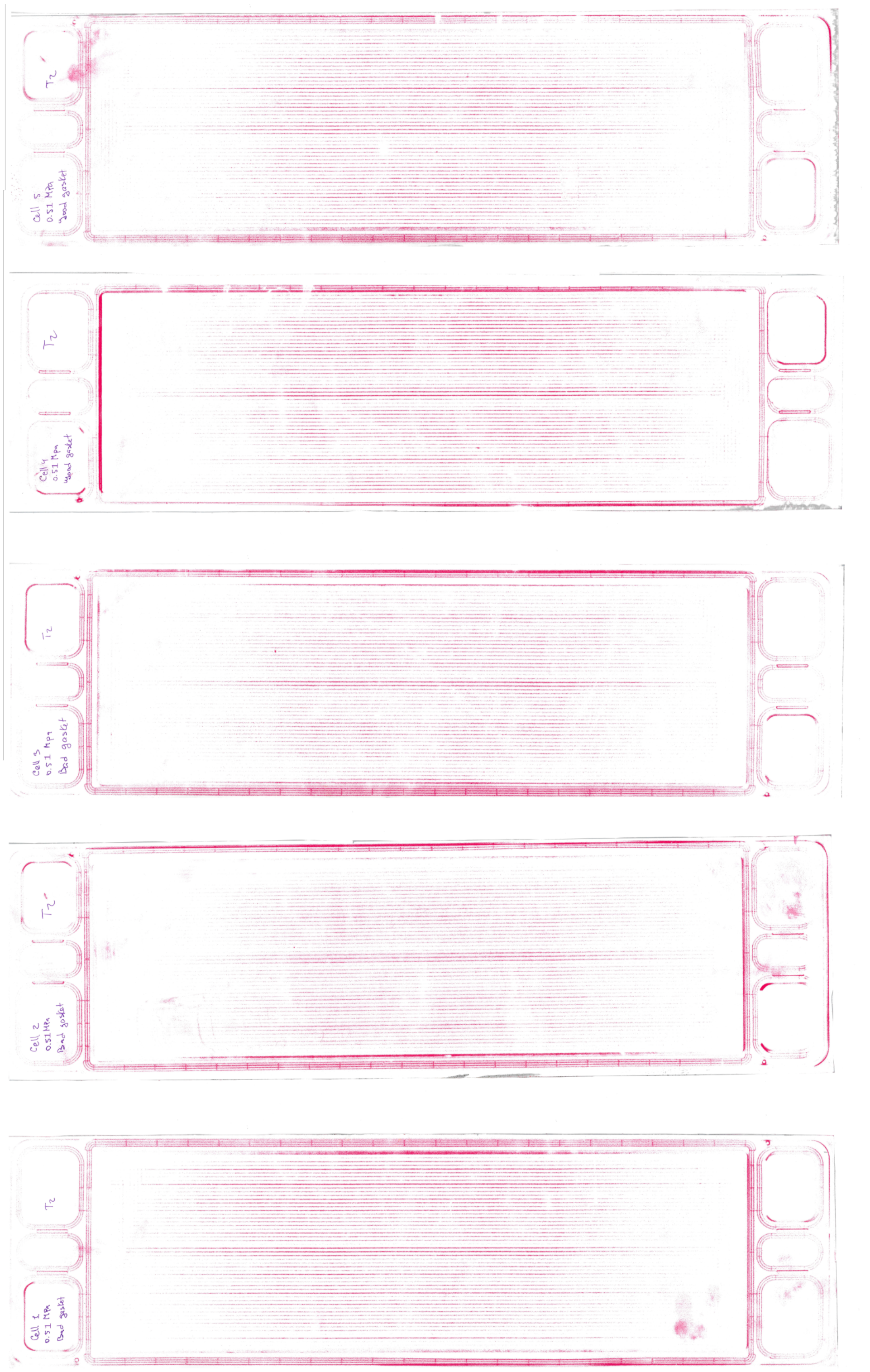

Figure 3.3: Third test using prescale film. Stack of 5 cells has been built. Each cell was measured individually one by one, starting from the bottom. 2 GDLs have been used. 2 batches of gaskets have been used: good and bad.

advantage of having higher percentage of cells with even clamping load distribution.

The only feasible reason for getting a leak in the middle of the stack is a damaged gasket or an error in the assembly of the cell and not due to uneven clamping load.

The far edges of BPP appear to have a lower load than the middle of the BPP. Which can explain the most common location of leaks, close to anode cathode inlets & outlets. In [16] [8] it is argued that optimising the design of end plates can vastly improve the load distribution on the cells in a stack and a different project with high capability for large scale 3D FEM analysis is required to successfully to achieve it on stacks from this thesis.

As to the difference in good and bad gaskets, it wasn't possible to observe any visual critical difference between these 2 groups of gaskets using prescale film.

3.2 Leak tight test on bipolar plates

When building stacks used for tests, bipolar plates must be quality checked by performing a leak test. Method of performing a leak test is described in the previous chapter. The results of those test are presented here.

The BPP were tested by the production, they changed hands, after the second leak test 20% failure rate of BPP was observed. Needing to acquire new BPPs resulting in a time and money loss.

The bad plates probably failed due to transportation from production to test facilities, resulting in stacks that couldn't hold even low amount of pressure. Changing the faulty BPPs resulted in stacks that passed the leak test and were further used for other intended tests.

Usually, the department that builds stacks doesn't have a long trip to retrieve the BPPs. All BPPs are pressure tested, and faulty ones rarely make it into the stack if they make it at all. The theory is this 20% failure rate of BPP can be attributed only to the test department that is located a short but extremely bumpy trip away.

There are several potential fixes for this problem. First solution is to improve the compound used in production of BPP giving it more ductile properties and reducing the range of stresses in which they can be damaged. Something, that is already being investigated by the material department and outside the scope of this thesis.

The second solution is quite cheap and requires less time to implement. Procure better transportation methods between departments that significantly limit the vibrations and shaking of the BPPs. Place BPPs in boxes with Styrofoam or alike material. Insight into the automation and factory layout will also result in a leaner process in the long run [27]. The test department at this stage of report has already been moved creating a leaner layout of the stack assembly process. It should minimise the number of broken and failed bipolar plates.

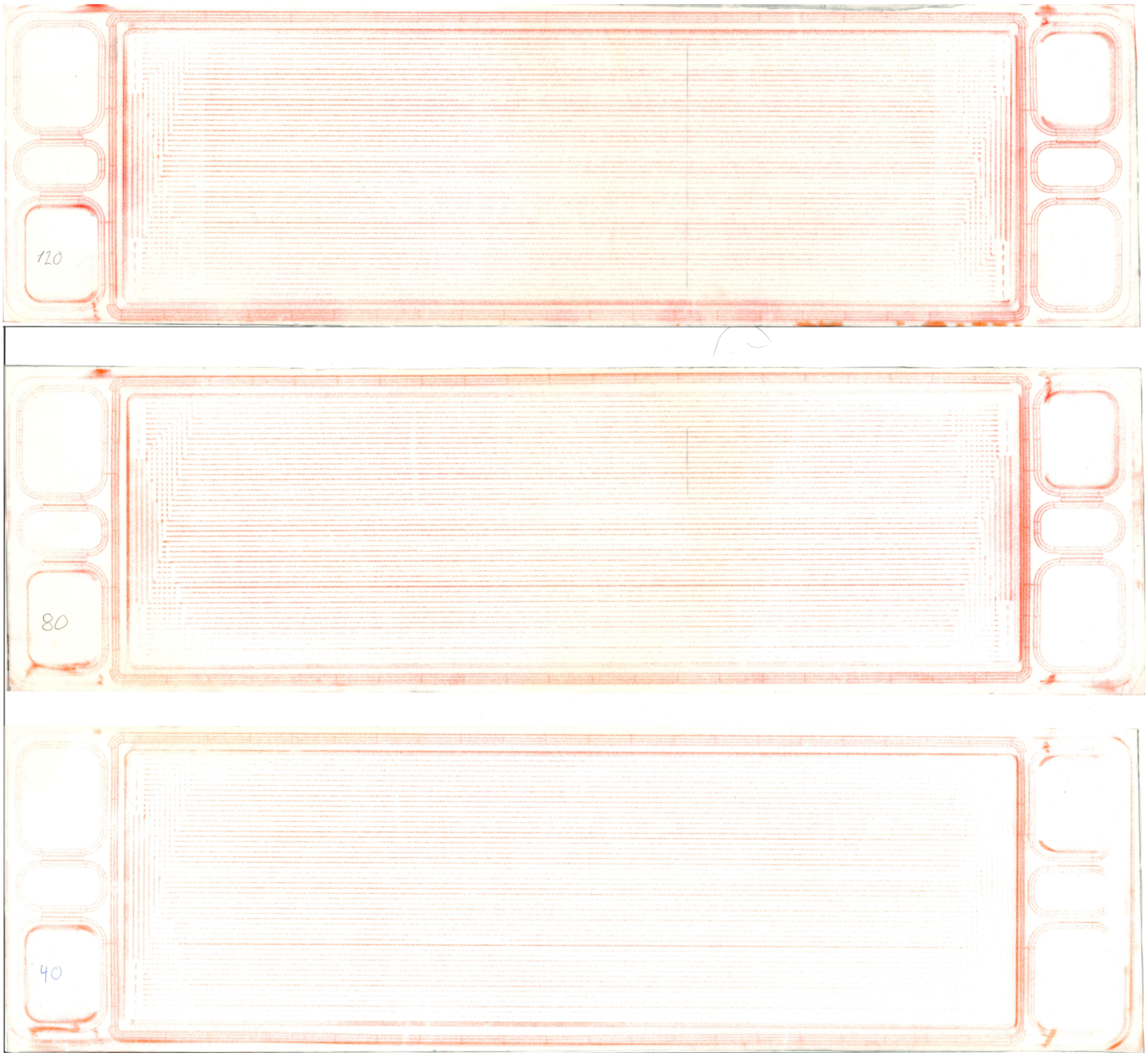

Figure 3.4: Clamping load distribution of a 160 cell stack. From bottom to the top, cell 40, 80, 120.

Chapter 4

Gaskets

The gaskets are most commonly responsible for faulty cells in a stack produced by the company. This chapter tries to find any visible and measurable deformations in the gaskets to determine the main cause behind their fault. Having an ideal clamping load is a recurring theme when analysing common mistakes in the stack assembly. So, it was investigated if the gaskets are being over compressed resulting in their failure.

4.1 Gasket tolerances

The design of the cell structure has a 0.35mm gap that allows the compression of a gasket before MEA compression. MEA should be also compressed by no more than 0.1mm, allowing the gasket to be compressed to a total of 0.45mm before maximum allowed compression is achieved as illustrated in the figure 4.1. Exceeding the 0.45mm compression would exert critical shear stresses on the MEA causing tears and irreversible physical damage. 0.45mm gasket compression will be referenced as ideal compression from now on.

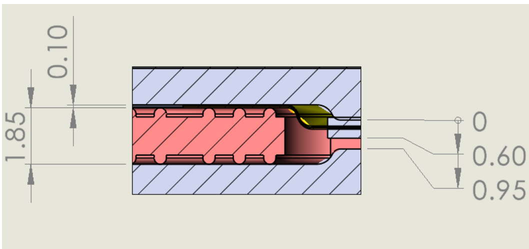

Figure 4.1: Detailed cross section of 1 cell, grey colour illustrates the BPP and red colour illustrates the gasket, yellow-gray sandwich illustrates the MEA. 0.1mm is the thickness of the sub-gasket. 1.85mm is the ideal gasket thickness. 0.6mm is the MEA thickness. From 0.6mm to 0.95mm (0.35mm) there is space to compress the gasket.

Table 4.1 shows a sample size of 10 gaskets from the original supplier. Gasket thickness was measured using a micrometre in the places shown in the figure 2.4a. The acceptable dimensions are 1.85±0.1mm. The average values with min and maximum and standard deviation are found in table 4.2 to be an average height of 1.82mm, maximum height of 1.9mm minimum height of 1.79mm with a standard deviation of 0.026. As it stands, the original supplier did produce the gaskets within the predetermined and accepted tolerances.

Technical design verification test template has been written and implemented with colour coding to test new received gaskets from now on. Colour coding will flag any gaskets that are not within the agreed tolerances.

Table 4.1: Gasket thickness measurements.

Gasket	Point 1	Point 2	Point 3	Point 4	Point 5	Point 6	Point 7	Point 8
1	1.88	1.83	1.8	1.81	1.85	1.8	1.79	1.81
2	1.84	1.81	1.81	1.81	1.85	1.82	1.79	1.81
3	1.85	1.81	1.8	1.8	1.85	1.84	1.8	1.79
4	1.83	1.82	1.82	1.84	1.89	1.81	1.8	1.8
5	1.89	1.83	1.81	1.83	1.84	1.83	1.8	1.83
6	1.85	1.81	1.82	1.82	1.87	1.8	1.8	1.8
7	1.9	1.8	1.81	1.83	1.87	1.83	1.84	1.82
8	1.88	1.8	1.8	1.81	1.83	1.8	1.8	1.81
9	1.85	1.81	1.81	1.83	1.86	1.82	1.8	1.82
10	1.86	1.8	1.81	1.82	1.86	1.82	1.81	1.81

Table 4.2: Gasket height statistics: average, standard deviation, max value and minimum value.

Average	STD	Max	Min
1.82	0.026	1.9	1.79

4.2 Microscope imaging

This section outlines the results from analysing the gaskets under a microscope. The main reason was to try and observe any visible deformations from bad gaskets and compare it to the new gaskets. Digital Dino-Lite Premier microscope was used with Dino-Lite 2 capture software.

4.2.1 1st microscope analysis

For the first attempt at microscope imaging, 3 batches of gaskets were selected: Batch 1 gaskets taken from faulty cells showing low voltage. Batch 2 gaskets from cells showing good voltage performance. Batch 3 gaskets were new unused gaskets. 1 unused gasket, 3 bad gaskets and 3 good gaskets were analysed.

They have been analysed in this order: New, Good then Bad gaskets. All points of interest have been photographed than analysed. The examples of most commonly observed deformations are shown in figure 4.2. It can be noted that new unused gaskets looked healthy and without any critical visible deformations with a small exception of slight mistakes in forming process that left a little bit of material removed from the gaskets across their lips, which is not considered a critical issue. While the bad gaskets had around 16 cuts per gasket which seems excessive.

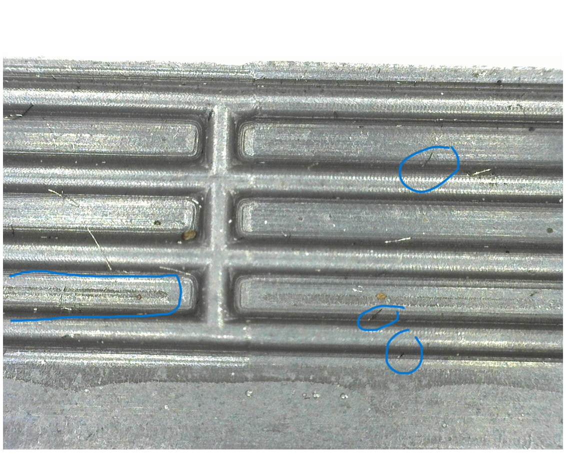

(a) Example of cuts across the gasket lips

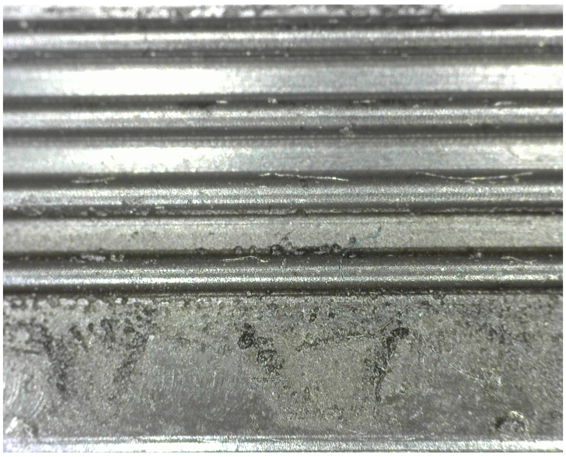

(b) Acid leaching from sub gasket leaving visible deformation on gasket sealing face.

Figure 4.2: Microscope images of examples of gasket deformation.

Good gaskets showed some deformations: cuts across the lips which are thought to be from overstretching the gaskets during the assembly, slight acid leaching from sub gasket have been also observed as well as small metal objects which were probably attached to the gaskets from the dust. A thing of note is that the gaskets were extremely dirty and had a lot of dust, dirt, fibers and human follicles on them. Higher standards of cleaning have been implemented during the assembly process. Assembly areas have been designated as dust free and new rules regarding work clothes have been implemented.

Same observations were made when looking at bad gaskets. Figure 4.3 shows the number of deformations seen on bad cell gaskets is almost 3 times higher than on the good cell gaskets. Higher number of deformations could be responsible for a higher chance of leakage of reactant gasses from the cell, also higher potential for gas cross flow, explaining the low voltage.

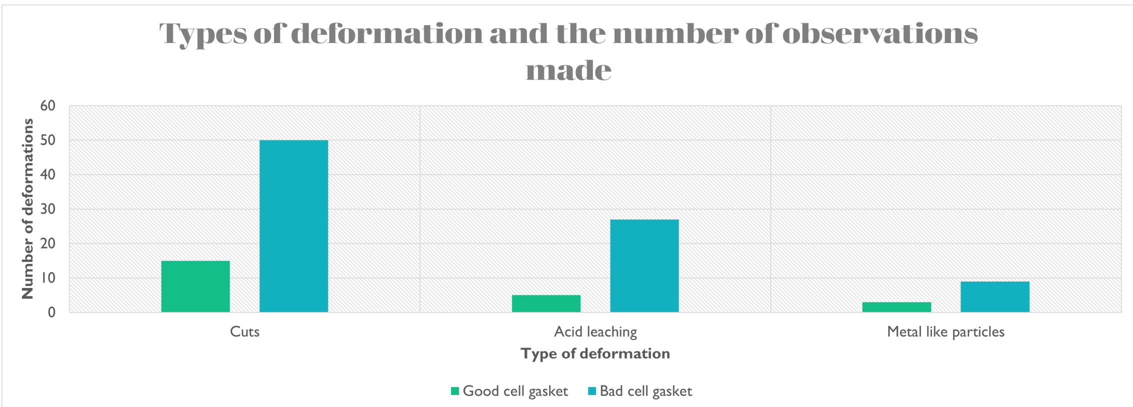

Figure 4.3: Results for microscope imaging, 1st attempt.

During the first experiment, the unknown factor was the origin of gaskets. it wasn't

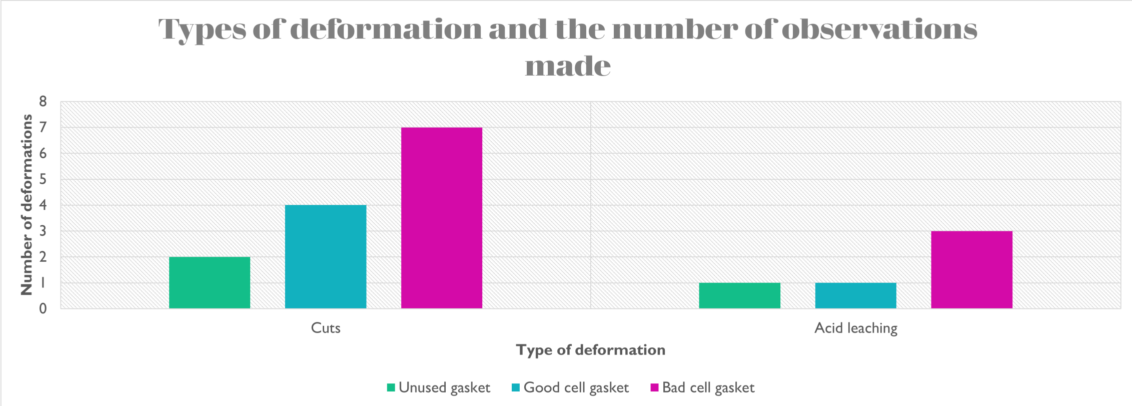

Figure 4.4: Results for microscope imaging, 2nd attempt.

known from which exact cell did they originate, or if those cells have been previously repaired. To remove this uncertainty and to ensure the knowledge the exact origin of gaskets a second experiment was proposed and performed. It had the exact structure as the first attempt, only for the second attempt the author was present for the repair, and noted the exact cell they came from and marked the gaskets to avoid any future confusion.

4.2.2 2nd microscope analysis

During the second experiment a total of 6 gaskets were removed from a 160 cell stack that ran for 80 hours for FAT. This stack had a new batch of gaskets that were 0.05mm thicker than previously due to tolerance errors. During the removal of gaskets, only 5 gaskets could be retrieved, 3 good ones and 2 bad ones. 1 gasket was fused with the sub gasket of the MEA. Under closer inspection, it was found that the MEA was assembled wrong resulting in a faulty cell.

The rest 5 gaskets were analysed under the microscope. The results are shown in figure 4.4. It can be seen that the while the previously seen deformations are also seen here, the nr of deformations has decreased to 3.5 cuts per bad gasket.

It is still possible to visibly several deformations under microscope on the gaskets. It is unacceptable and should be investigated further. 2 types of deformations seen are chemical and tear. A long-term thermal test in phosphoric acid solution is recommended to be performed on the gaskets to give a better insight into the material's stability under high temperature and acidic environment.

To increase the durability of the material a different gasket shape design was researched in the next chapter. The goal was to reduce the stiffness of the gasket by changing the design. Making the gasket softer is assumed to make it more resilient to cuts and improve the sealing. Distributing the stresses more evenly will also move the stress points away.

4.2.3 3rd microscope analysis

The second microscope experiment showed a predominant amount of cuts and defects in failed gaskets. The working theory was that the cuts appeared either from overstretching the gasket or from over compressing them. At some point during the compression, the gasket is probably being over compressed and allows the over-compression of the MEA leaving an imprint. That could also pose reduced performance as over compression usually results in reducing the porous environment of the GDL [8] preventing the optimal gas travel and increasing the internal resistance.

As the next step, for the third experiment, it was decided to test new gaskets, and compress them with an increasing clamping load with an increment of 2,453 N. The gaskets were compressed to the required clamping load, left for 10 minutes then marked down before being analysed. After testing 10 gaskets, it appears that gaskets start to form cuts after increasing the load from the nominal 19,620 N. Increasing the force to 24,525 N results in an increased number of observations of the cuts in the gasket. Below 19,620 N there were no deformations observed. Force 22,073 N resulted in 1 cut and 24,525 N in 3 cuts. Even though higher compression resulted in a few cuts on the gasket, it can't be argued to be the only reason for a huge number of cuts on the gaskets removed from the failed cells.

4.2.4 Gasket cross section

During the microscope imaging it was found that the gaskets look a little bit off from technical drawings. Gasket cross section was cut and was found to be different as the lips had fillets instead of being under a 90°angle. Images from microscope were loaded into Solidworks and differences were measured. Next chapter shows the results of FEM analysis using the cross section of the gasket that is asked to be produced vs gasket that is actually being produced. Figure 4.5 was made at the later stage of this project, when a different supplier delivered their batch of gaskets. Gaskets from supplier nr 2 appear to respect the technical drawings.

4.3 Gasket and MEA compression

To determine the optimal clamping force needed for ideal compression of a gasket and the MEA, 2 different stacks have been assembled. One stack consisted of 20 BPPs and 21 gaskets and a different stack that consists of 21 BPP and 20 MEA as shown in figure 4.6. Both stacks have been compressed with an increment of 981 N, starting with 0 N until at least 19,620 N could be reached. Due to high MEA stiffness, and instability of the hydraulics press, it was difficult to reach higher compression forces. At each increment the stack heights were measured as shown in figure 2.5. The results have been used to analyse the deviation from tolerances of the gaskets and calculate the stiffness of the MEA and gasket. Results for gasket and MEA compression rate under different forces are presented in the figure 4.7.

Gasket and MEA stiffness were calculated using Hook's Law [28] shown by equation 4.1

(a) Cross section of the gasket from original supplier, referred as supplier 1 in this image.

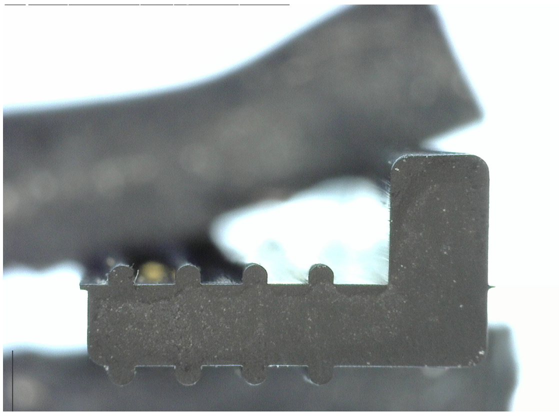

(b) Cross section of the gasket from a different supplier, referred as supplier 2 in this image.

Figure 4.5: Cross section of gaskets from different suppliers analysed under the microscope.

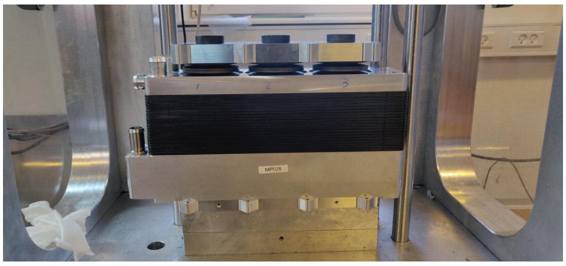

(a) Stack build out of BPPs and gaskets to test the gasket compression over different clamping force.

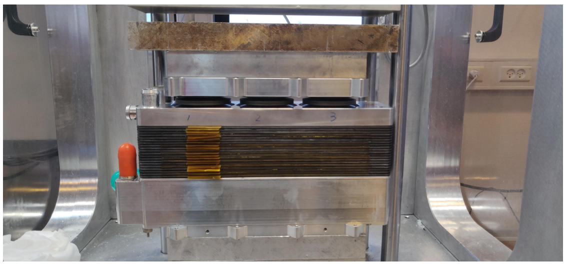

(b) Stack build out of BPPs and MEAs to test the MEA compression over different clamping force.

Figure 4.6: Stacks build to test compression and stiffness under different clamping load.

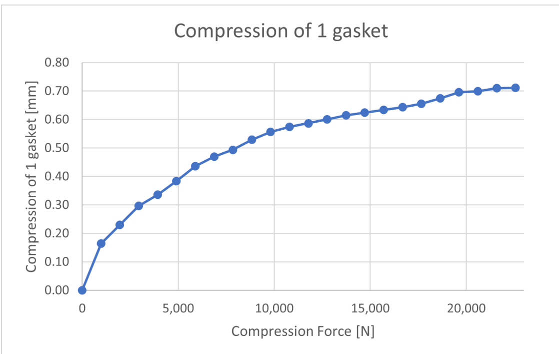

(a) Averaged compression of 1 gasket after measuring the stack compression under different forces.

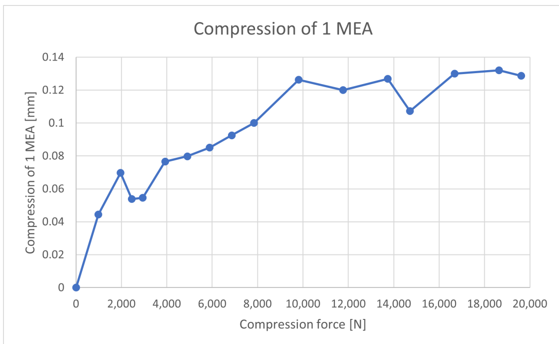

(b) Averaged compression of 1 MEA after measuring the stack compression under different forces.

Figure 4.7: Compression of 1 gasket and 1 MEA after building 2 stacks with only gaskets and only MEAs.

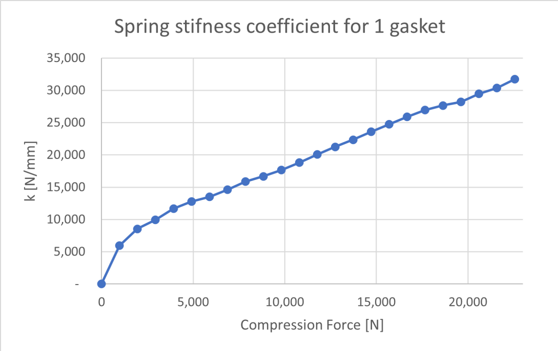

(a) Gasket stiffness calculated from the figure above using Hook's law for each 981 N step.

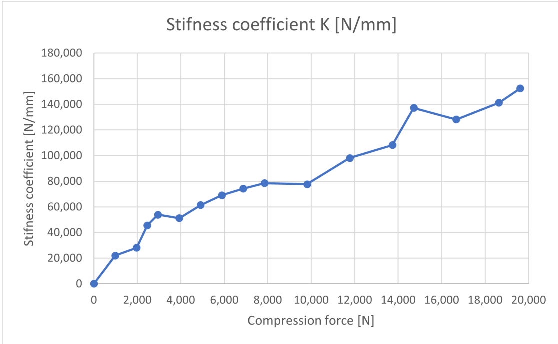

(b) MEA stiffness calculated from the figure above using Hook's law for each 981 N step.

Figure 4.8: Stiffness diagrams for normally used gasket and MEA.

using the data shown in figure 4.7. Hook's Law is used for linear materials. Because both MEA and Gasket are nonlinear materials the stiffness was calculated at each point of compression making it accurate for 981 N increments. The results are shown in figure 4.8.

MEA compression and stiffness appear to have small errors in the diagrams, as in real life it doesn't decompress and doesn't become softer sporadically. The errors can be attributed to the measuring errors as the difference in measurements between 2 steps is similar to the error of measurement. Due to the design of the hydraulic press taking accurate measurements wasn't easy as well. Even using 20 MEAs in the stack setup wasn't enough to make a better plot. Better test setup is required where it would be easier to take height measurements at different clamping forces in the future.

$$F = -k * x \tag{4.1}$$

4.4 Clamping load vs stack performance

Both gasket and MEA stiffness were calculated and shown in figure 4.8. From technical drawings and 1 cell design shown in figure 4.1 the ideal compression force is shown in figure 4.10a to be 13,734 N. It was done by superimposing the compression of gasket and MEA into 1 graph. Knowing the tolerances for gasket thickness as 1.85±0.1mm the graph has been modified to reflect if a stack would be build using 1.75mm gaskets or 1.95mm gaskets as seen in figure 4.9. As it wasn't possible to measure all gaskets and pick and choose their dimensions only one ideal gasket compression load is used of 13,734 N from now on.

To test this theory a 10 cell stack was build shown in figure 4.10b. At first it was tested to be leak tight at 4,905 N. As mentioned in the previous chapters it was decided to compress it to a wide range of compression loads, then draw a polarisation curve under each clamping load, then compare the stack performance between clamping loads.

While 4,905 N was tested to be leak tight, it leaves a very narrow margin for error,

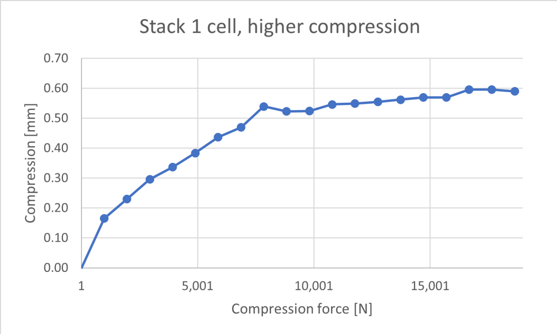

(a) Calculated ideal compression force of a stack when gaskets with +0.1mm tolerances are used.

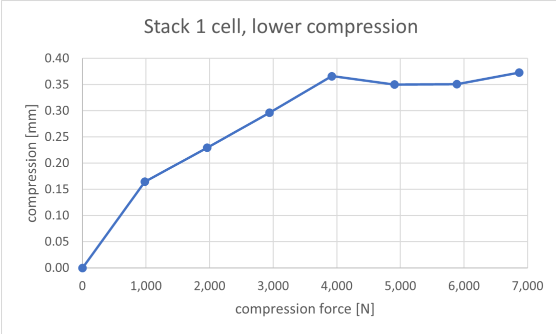

(b) Calculated ideal compression force of a stack when gaskets with -0.1mm tolerances are used.

Figure 4.9: Diagrams for ideal clamping force depending if the gaskets used are build within the lower or higher tolerances.

which is why the first clamping load to be tested was decided to be 9,810 N, then the calculated ideal 13,734 N, 17,658 N then 19,620 N which is the normal clamping load used in the production then 22,073 N and 24,525 N to visualise what happens when extreme overcompensation is applied.

Figure 4.11 shows the results of this experiment. The x-axis represents the clamping force in newtons, and each line shows the voltage that is drawn for a separate current density. On lower current densities the difference in the voltage that can be drawn from the stack when increasing the clamping load is minuscule lower than 10mV. The voltage does start to improve on higher current densities, starting from 0.4A/cm2 with an improvement of 10mV and an improvement of 20mV at 0.8A/cm2.

For low current densities the ideal clamping load can be close to 15,696 N while for the higher current densities is in the range of 17,658∼19,620 N. Because these stacks should be able to operate at any current density, they will not be built to operate at a specific current density. So, it doesn't make sense to build these stacks at an optimised clamping load for each current density.

Gasket thickness tolerances are 1.85 $\pm$ 0.1mm. The thermal expansion of the gaskets noted by the supplier is up to 2% at higher temperatures. Which doesn't explain the big difference from ideal compression when comparing to experimental data. Next time when this experiment is repeated, the thickness of the stack should be measured before compression at room temperature, after compression at the room temperature and while still hot after operation to note the difference in gasket compression. One possibility is that the gaskets are expanding at a higher percentage than stated by the supplier. Moving the ideal compression load higher, bringing it closer to the range of 17,658∼ 19,620 N.

As it stands now, with the available experimental data it is suggested to lower the clamping load to 17,658 N and run a long term test on its stability.

The performance keeps improving though with increasing the clamping force. The stack hasn't yet reached the peak where its voltage would start to decrease. Because increasing

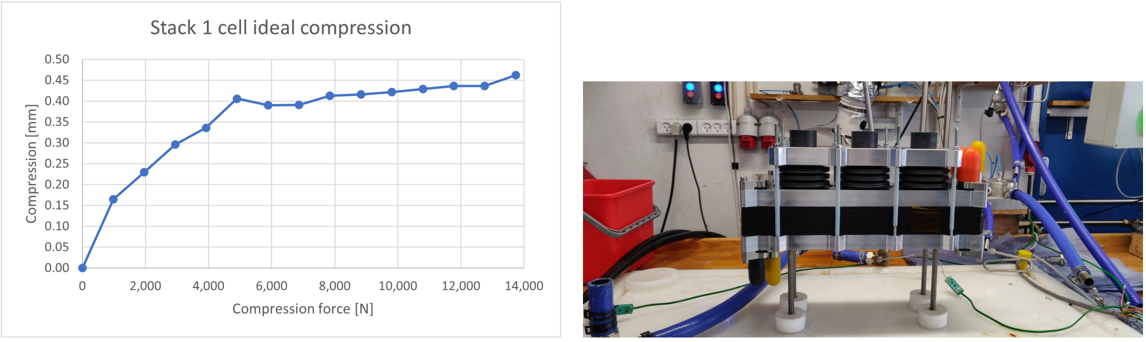

(a) Compiled compression of gasket and a MEA to illustrate the ideal force compression. Left part of the graph shown the compression of the gasket until 4,905 N, the right side shows the compression of both gasket and MEA until 13,734 N compression clamping force is achieved.

(b) Stack build for testing the influence of different clamping loads on the voltage and current performance of the stack.

Figure 4.10: Validation for building a 10 cell stack under various clamping loads to test its performance.

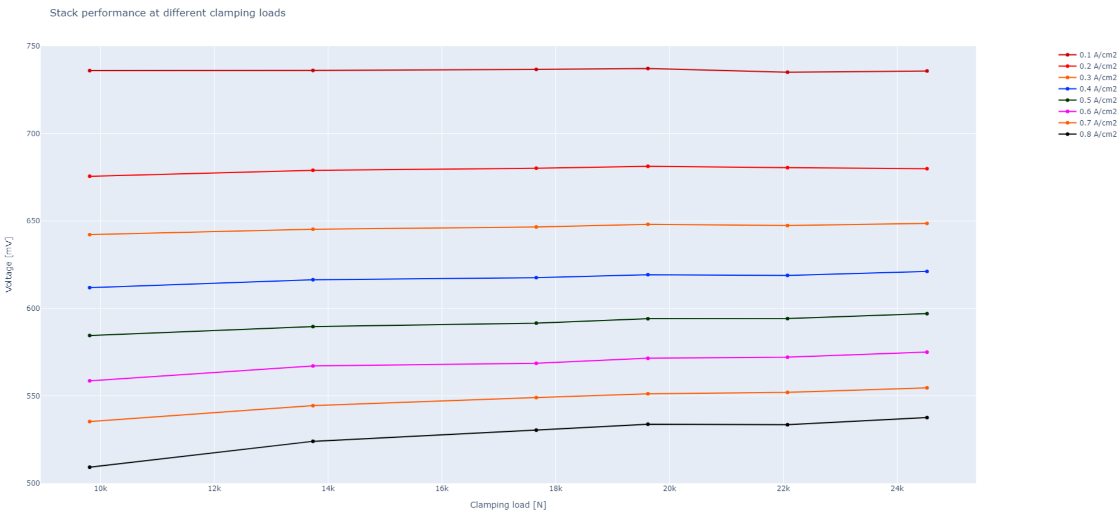

Figure 4.11: Graph of voltage at different clamping loads. Each line is represented by 1 value of current density.

the voltage is a priority for the company, this experiment is still ongoing to gather more data into improving the stack voltage.

Chapter 5

Finite Element Method analysis

For this FEM simulation a modest laptop was available with Intel(R) Core(TM) i7-8850H CPU @ 2.60GHz 2.59 GHz, 32GB of 2667 MHz RAM and Nvidia Quadro P2000. The goal of Finite element analysis was to analyse the gasket for its stability during deformation, stress distribution and calculate its stiffness. The results have been used to improve the design of the gasket to a less stiff gasket by manipulating its shape.

5.1 3D FEM analysis

For 3D FEM analysis simplified geometries were created from CAD files as shown in figures 5.1, 5.2. Unfortunately, due to limitations of the student license with a maximum allowed nodes and element number, an acceptable mesh couldn't be achieved resulting in skewed and untrustworthy and plain wrong results. The main cost of achieving these wrong results was lost time.

Which is why the focus has been shifted to 2D analysis using a simplified geometry to save on computational power and time used for each simulation that went from half an hour to a few minutes. Considering that not all simulations were successful those half hour failures accumulated into days without any results. Using simple 2D geometry allowed to fail fast and find converging models quicker.

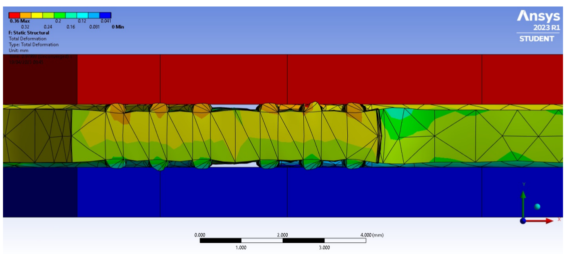

(a) Simplified 3D geometry initial results, side view.

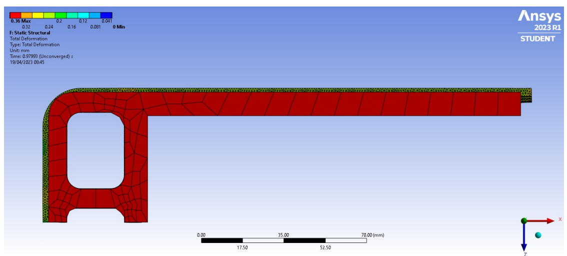

(b) Simplified 3D geometry initial results, top view.

Figure 5.1: Results for simplified 3D geometry of 1 cell sandwich. Instead of BPP monopolar plates are used. 5.1b 1/4 of a cell is considered, without considering the channels and ribs of BPP.

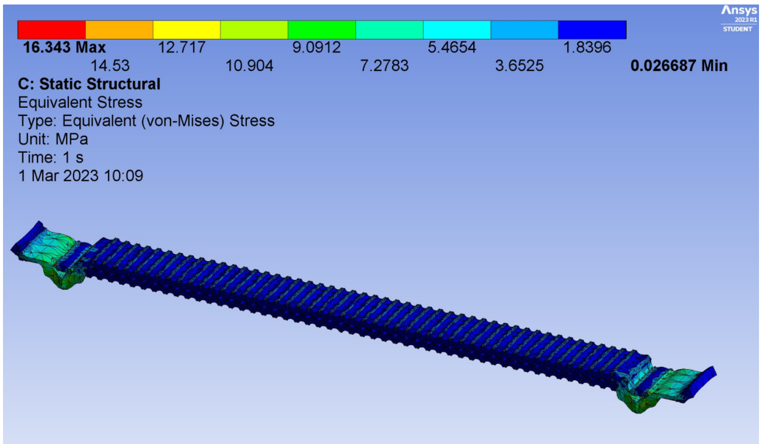

Figure 5.2: 10 mm cutout of 1 cell assembly.

5.2 2D FEM analysis

For 2D analysis, nonlinear mechanics and hyper-elastic materials have been used. CAD models have been redrawn in Solidworks as 2D planes consisting only of 2 monopolar plates and 1 gasket between them. For material properties 2 primary materials were created. Bipolar plate material data was used from available data from the company. Gasket material property was constructed from hyper-elastic material available in the Ansys database using Mooney-Rivlin 5 parameter curve that was fitted to real data gathered from the experiment results shown in figure 4.8.

It was achieved by dividing the stiffness by the perimeter of the gasket to achieve the stiffness of 1mm width of a gasket, as 2D simulation has a 1mm thickness by default.

Due to hyper-elastic properties of the gasket, nonlinear model was used with adaptive re-meshing of the gasket [29]. Iterative process was used, with minimum allowed step number of 100 and maximum of 1,000 to ensure the best convergence [30].

Figure 5.3 shows the initial designs of gaskets that were considered in the simulation. During original microscope imaging of gaskets, it was noted that the design of gaskets is deviated from the technical drawings. Cross section of gasket was cut, photos were taken using a microscope of the cross section. Images were imported to Solidworks and the real dimensions were reverse engineered. The real gasket design is called V1. V2 is the original design that stays true to technical drawings. V3 is a slightly modified version of V2 with small fillets in the corners. V5 and V6 are more drastic design changes proposed to reduce the stiffness, dissipate the stresses more evenly across the gasket, improve the slip of gasket during the compression and force it to be squeezed more equally in all directions. Numbers 0.3, 0.35 and 0.4 in the name of each version stand for gasket lip height.

After initial simulations the data has been gathered into the figure 5.4. The real data wasn't exactly close to the simulation results. The curve was following the same shape, which meant that after a little bit of adjustment of Ansys material database it would get

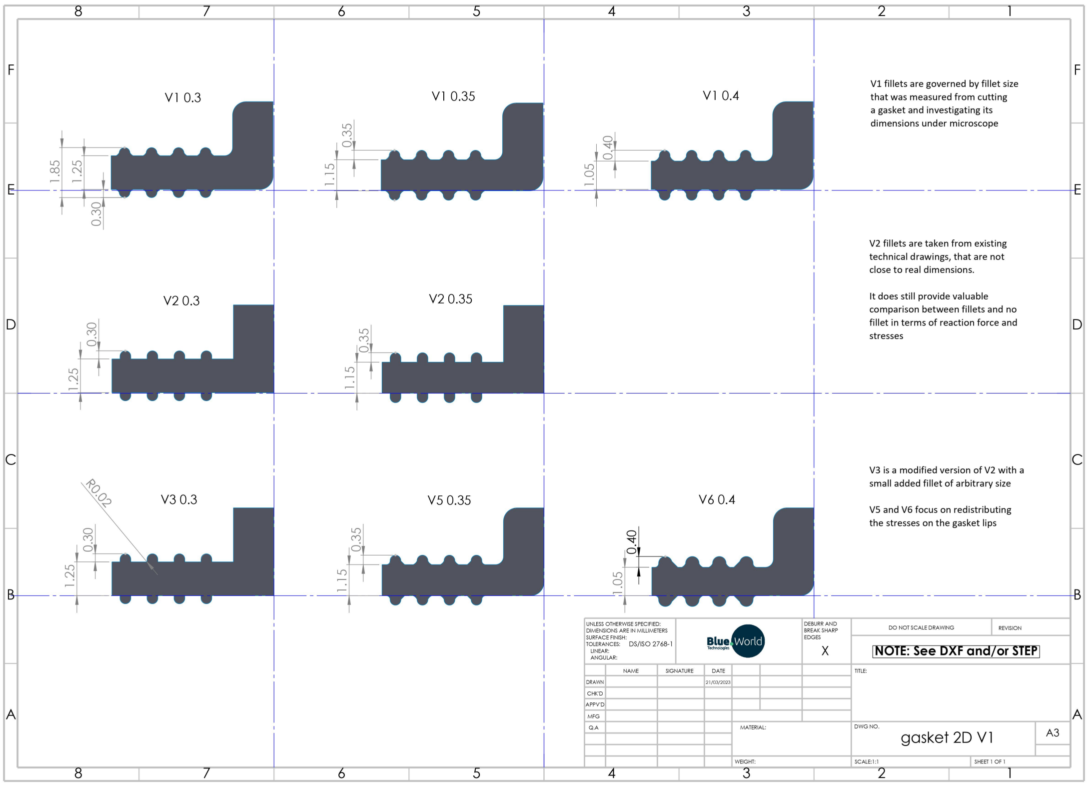

Figure 5.3: Technical drawing illustrating the key differences between various design choices for FEM analysis.

closer to real life gasket hyper elastic properties as seen in figure 5.5, where the real data is shown with black colour.

An interesting difference in deformation, stress distribution and stiffness could be observed between the V1 and V2 versions of the gasket. Figure 5.5 shows V2 to be 7.7 % less stiff than V1. A big difference was noted between the requested V2 and what is actually being produced V1, resulting in a stiffer and less superior gasket. Investigation has been started to look into the quality issues of the supplied gaskets.

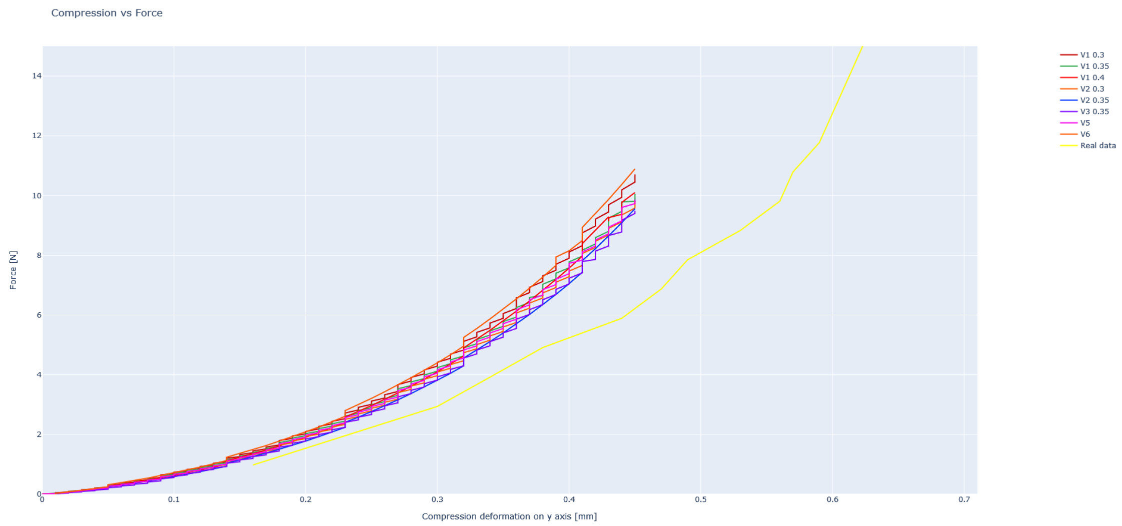

Figure 5.4: Force vs compression curve of all simulations, before fit to real data.

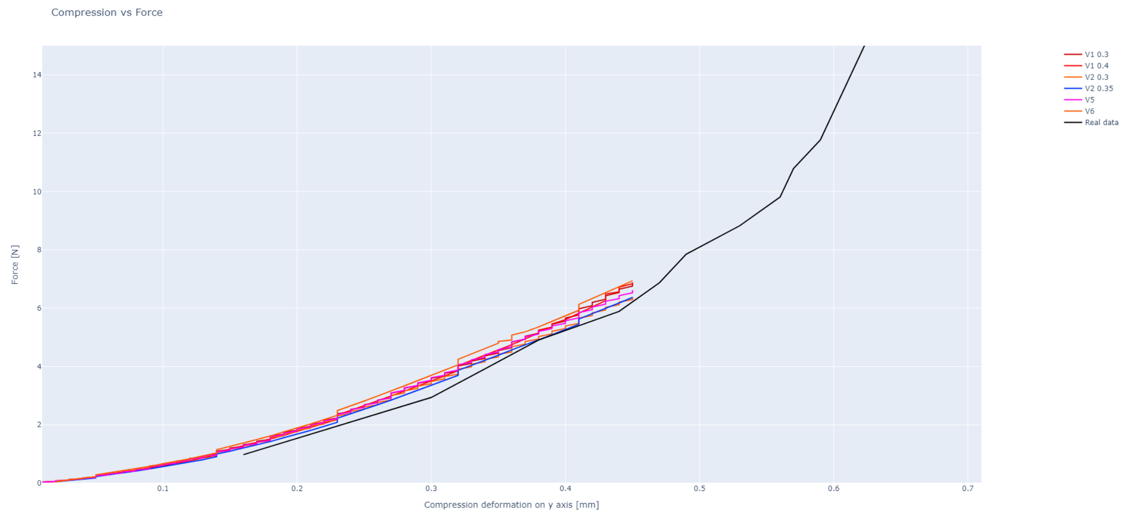

Figure 5.5: Force vs compression curve of all simulations, after fitting hyper-elastic material properties to real data.

Figures 5.6 and 5.7 shows zoomed in stress distribution in V1 and V2 version of the gasket. It shows that V2 stresses are higher than in V1, and V1 looks to have weak points in the corners of the lips. Preliminary analysis is that in V2 tears should start to appear in the corners of the lips. While in V1 it looks like the top of the lips will be the first to fail and create cuts in the material. V1 on the other hand looks to have a better stress distribution than V2. Probably due to bigger area of effect on which the forces are distributed. See equation 2.1, the higher the area the lower the stress.

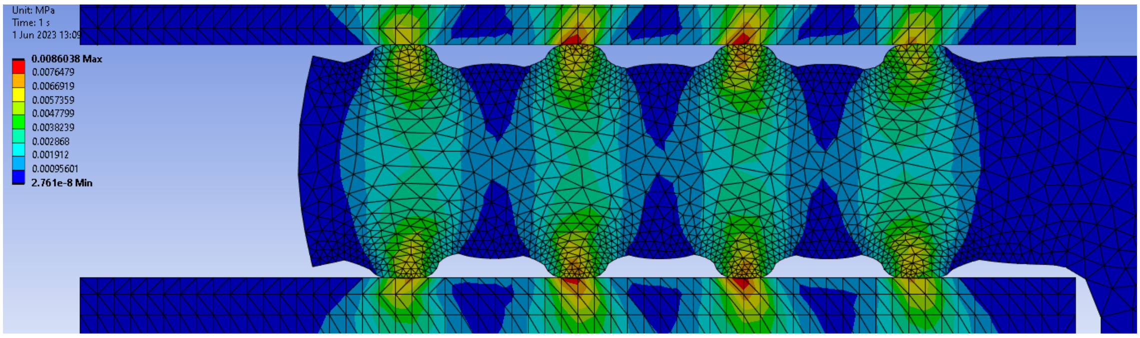

Figure 5.6: V1 0.3 Von-Misses stress. Used for comparison of final designs. Units in MPa.

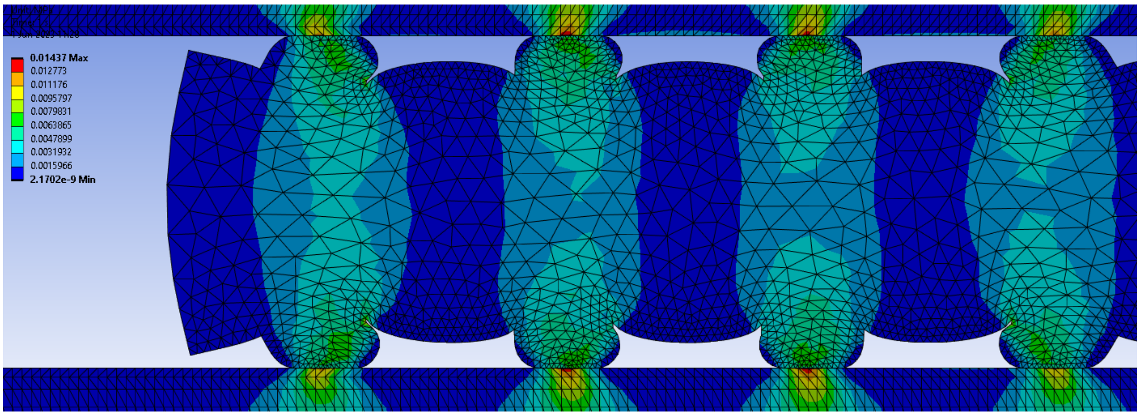

Figure 5.7: V2 0.3 Von-Misses stress. Used for comparison of final designs. Units in MPa.

5.2.1 Final redesign

For final proposed design change, the best previous design was chosen as V5, then multiple versions of it were created with small changes to optimise the stiffness and stress distribution. For the final version, a more complex BPP was included with the gap for one of lips. The mesh of these designs can be seen in figure 5.8. During the previous simulations, gasket slippage out of cell was noted. The final redesigns as shown in figure 5.9 also improved on the slipping effect of the gasket. V5.8 shows an almost zero slip, while V5.7 shows a small slip.

A lot of gasket slippage is happening due to the elastic nature of the gasket, as it needs space to be squished out, as the BPP doesn't prevent it, it slips outside the BPP. V5.8 takes more advantage of the small channel in the BPP to force the gasket 4th lip to make contact as soon as possible with the channel during the compression, helping the gasket to stay in its place more firmly.

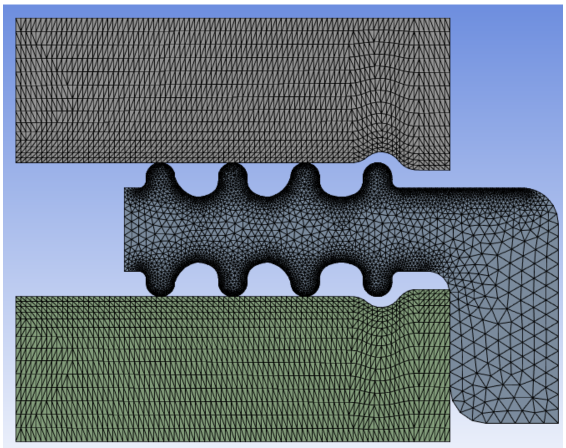

(a) V5.7 mesh all triangles.

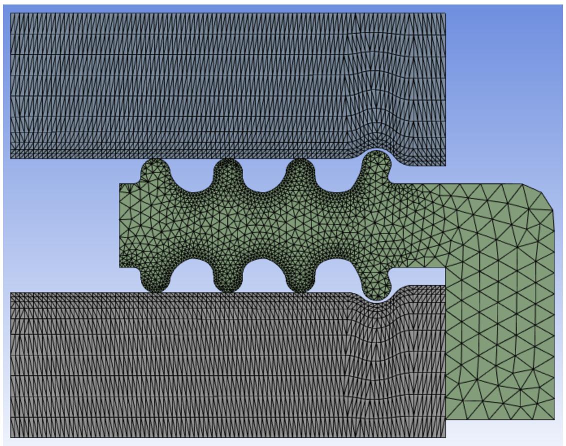

(b) V5.8 mesh all triangles.

Figure 5.8: Mesh comparison of 2 final designs. Final versions were refined to use all triangle mesh with smaller size of triangles than in previous simulations.

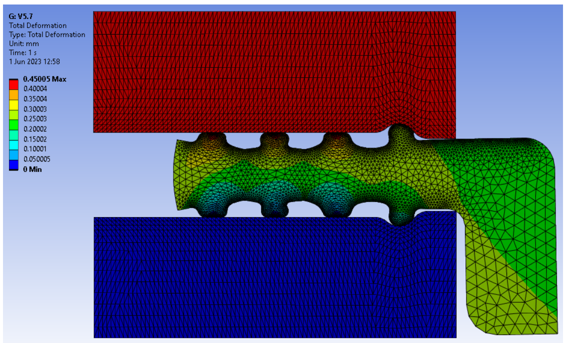

(a) V5.7 deformation overview.

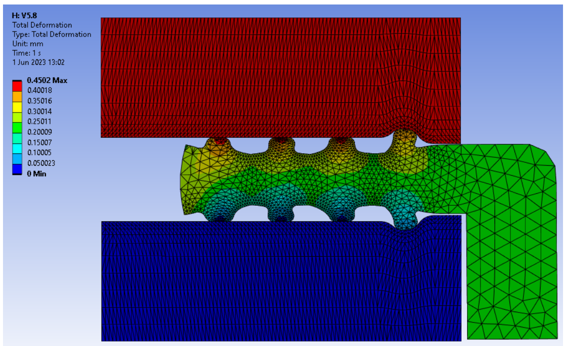

(b) V5.8 deformation overview.

Figure 5.9: Deformation comparison of 2 final designs.

To take advantage of working on the final designs, mesh was refined from 0.43 to 0.3mm with new mesh shown in figure 5.8 and mesh statistics shown in 5.10. A smaller edge sizing of 0.01mm was used to achieve a finer mesh. Mesh was changed from a mix of triangles and squares to only triangles. Using only triangles while gives a more accurate result, also takes longer to compute. It done at a later stage to refine the final results with a bigger time cost that could be ignored at the final stage of the project. The mesh quality could be improved even further for future work, if a more powerful computer will be available that has more processing power. Improving the mesh and choosing an even smaller particle size would give even more accurate results.

Statistics	
Nodes	7180
Elements	13212
Show Detailed St...	No

(a) V5.7 mesh statistics.

Statistics	
Nodes	3657
Elements	6522
Show Detailed St...	No

(b) V5.8 mesh statistics.

Figure 5.10: Mesh statistics comparison of 2 final designs.

Figure 5.11 and 5.12 shows Von-Misses stress in the final redesigns. The stress distribution was optimised so that the stresses travel to both left and right side of the gasket lips, not just focus on one of the sides as shown in the figures 5.6 and 5.7. When comparing to V2 The stresses also decreased as the acting forces were affecting a larger area. The exact centre of the lip is experiencing the highest stresses, not lip edges and corners as in V2. The centre of the lip being the strongest point, and the corner of the lip the weakest point it shows an improvement of changing the location of stresses.

As seen in figure 5.6 stress distribution is not everything as those gaskets still failed a considerable amount of time. The outcome is that all previous tests should be repeated with the new gaskets from supplier 2.

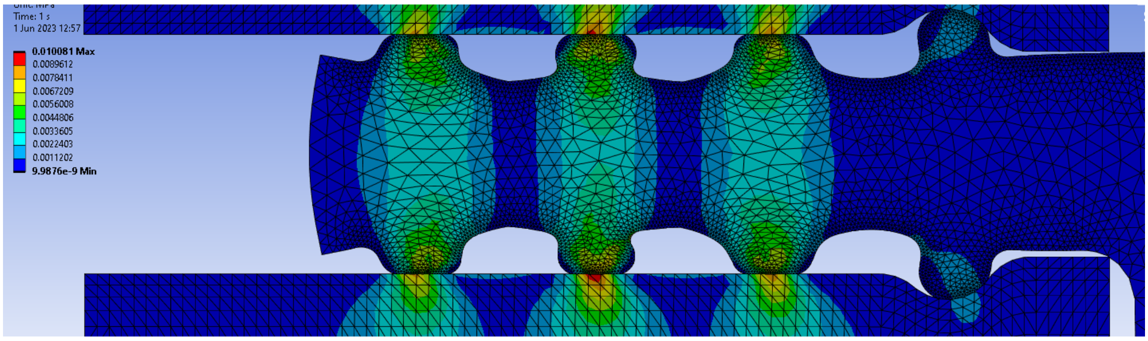

Figure 5.11: V5.7 Von-Misses stress. Units in MPa.

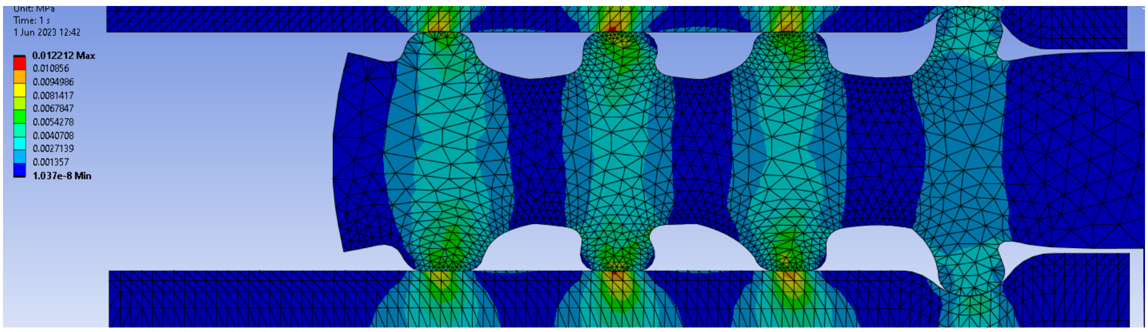

Figure 5.12: V5.8 Von-Misses stress. Units in MPa.

Figure 5.13 and 5.14 show the convergence of the final simulations. It is shown as proof that the simulations have been solved. V5.7 reached a viable solution in 490 steps and

V5.8 in 317 steps. It also shows that mesh was re-meshed several times when the convergence of matrix stiffness was struggling. This feature of re-meshing and knowing the number of iterative steps together with the convergence was of great help to guess the initial mesh parameters. This graph was always consulted when the simulations weren't converging.

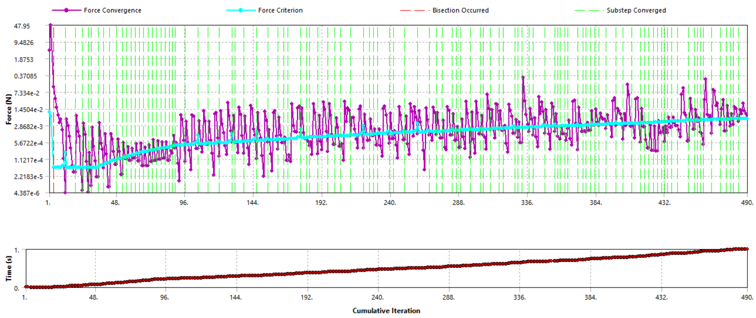

Figure 5.13: V5.7 convergence and re-meshing points.

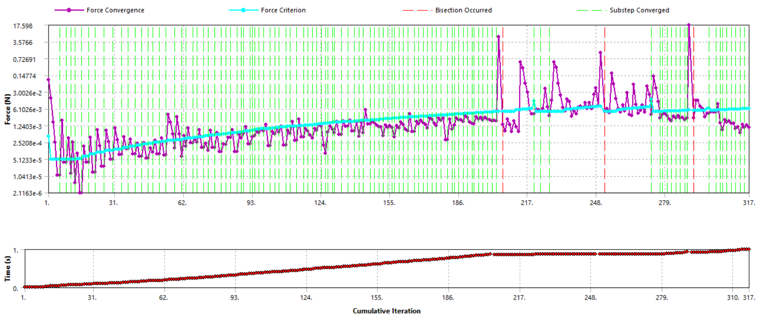

Figure 5.14: V5.8 convergence and re-meshing points.

Final results are presented in the table below. It shows that the V5.7 is an improvement in regard to gasket stiffness when comparing to the V1. V5.8 has an even worse stiffness although the gasket slippage has been drastically improved in this design. These 2 new designs can be the groundwork for another design that integrates both a softer design and improved slippage. As it stands now, gasket stiffness is a more important aspect than gasket slippage, so V5.7 is recommended as the next gasket design.

Table 5.1: Comparison of Force reaction on y-axis for original gasket to the final 2 designs.

	Original gasket	V 5.7 Gasket	V 5.8 Gasket
Y-axis Force [N]	6.87	6.35	7.45
% change in F[N]	-	-7.6%	+8.4%

Chapter 6

Conclusion

Based on the discussions made in this report its main findings are presented here.

Too high of a clamping load can reduce the porosity of the GDL lowering the overall performance of the stack. The clamping force vs stack performance test was of great interest and showed that the 19,620 N is close to being optimal. It could be seen that the voltage kept going up with a clamping force of 24,525 N by a few mV. This experiment is still ongoing with an even bigger compression force. The breaking point will be found when the voltage will start to decrease, this clamping force will be noted later.

There is a risk that increasing the clamping force even further, while improving the overall FC performance will negatively affect the lifetime of the stack. Long term tests should be implemented to compare the lifetime of the stack at clamping forces of: 17,658 N, 24,525 N and 27,468 N at minimum.

It was proposed to reduce the clamping load to 17,658 N and test its effect on long term stability of the stack. This experiment is ongoing with a higher clamping point to find the breaking point of the stack when the voltage will start to decrease. The stack hasn't yet reached the end of life and the results of this experiment might change the new recommended clamping load of 17,658 N.

Regarding improving the first pass yield and the quality of stacks assembled:

1. Failure modes of gaskets have been analysed, and discrepancy in the technical drawing and real life gaskets have been found and investigated. Design Verification Test template for quality control of gaskets has been written and implemented to compare gaskets from different suppliers.

   Gaskets from supplier nr 2 appear to respect the technical drawing from which they are produced and should be investigated in the next stack build to detect any difference in first pass yield.

   As shown in FEA, original gasket design was shown to be superior to the ones that were actually supplied. Based on FEA, slight improvements were proposed to the gasket to reduce the stiffness by 7.6% and mitigate gasket slippage. Even though the V5.8 shows better mitigation of slippage, it is much stiffer than the V1 version, which is why V5.7 is recommended to be tried out as the next possible design.

2. Quality issues were found in the test set ups that required some experiments to be repeated at least a few times. Oil leaks was a common occurrence, and improper components were used by accident. A leaner layout of the working area is suggested with better test set ups.

3. After analysing components under microscope the working place was found to be dirty. Higher standards of indoor climate have been proposed and implemented. The effect of air quality is being monitored daily and stricter rules regarding allowed work clothing has been implemented. Before it can be concluded that these

measures will result in an improvement, more time must be spent monitoring air quality. Subsequently it was decided to be tracked daily for an indefinite period of time until more results can be achieved.

6.1 Future work

New gaskets became available right before the end this thesis. Long term tests must be repeated to prove that the original design was superior to the one delivered by the supplier before. Using more correct gaskets might improve the first pass yield in the future.

An important aspect of the BPP is its high electrical conductivity which can be altered by different clamping load. Measuring the impedance during the compression vs performance can give an insight into the resistances of the BPP. A few researchers have made FEM simulations that predict contact resistance between BPPs and GDLs under even and uneven contact pressure distribution. This new research could be later used in further optimising the clamping load distribution by either changing the design of end plates or bipolar plates or both.

To further investigate the effect of the even clamping load distribution on the stacks, a 3D FEM analysis is required on the stack with multiple cells. Simplified 1 cell geometry using 1 stiffness coefficient for the whole cell can be integrated to reduce the computational time as done in ref [31]. Additional insight can be gained into the effect of clamping load distribution on the end plates leaving room for optimising the design by reducing the weight and making the structure more robust.

While working on optimising the design of the EP, a mini project can be done that investigates the pretension of bolts. When an ideal clamping load is known, having control over pretension of bolts and choosing 1 pretension value and using a torque wrench will improve the repeatability of the stack assembly narrowing the margin of error.

Bibliography

[1] *How Many Cars Are There In The World in 2023? Statistics by Country.* URL: https://hedgescompany.com/blog/2021/06/how-many-cars-are-there-in-the-world/.

[2] *Fuel types of new cars: battery electric 11.9%, hybrid 22.6% and petrol 37.8% market share in Q3 2022 - ACEA - European Automobile Manufacturers' Association.* URL: https://www.acea.auto/fuel-pc/fuel-types-of-new-cars-battery-electric-11-9-hybrid-22-6-and-petrol-37-8-market-share-in-q3-2022/.

[3] *The basic facts. How do the emissions of ships and cars really compare? - CE Delft - EN.* URL: https://cedelft.eu/publications/the-basic-facts-how-do-the-emissions-of-ships-and-cars-really-compare/.

[4] Hannah Ritchie, Max Roser, and Pablo Rosado. "CO and Greenhouse Gas Emissions". In: *Our World in Data* (May 2020). URL: https://ourworldindata.org/co2-and-greenhouse-gas-emissionshttps://ourworldindata.org/emissions-by-sector.

[5] *A future for hydrogen in European transportation.* Feb. 2020. DOI: 10.1038/s41929-020-0438-9.

[6] *Hydrogen engines to be mass produced by Hyundai by 2025 - H2 News.* URL: https://www.hydrogenfuelnews.com/hydrogen-engines-hyundai/8557564/?saved=true&form_id=57416&render_id=0.

[7] Wenming Huo et al. "Elucidating non-uniform assembling effect in large-scale PEM fuel cell by coupling mechanics and performance models". In: *Energy Conversion and Management* 277 (Feb. 2023). ISSN: 01968904. DOI: 10.1016/j.enconman.2023.116668.

[8] C. W. Wu et al. *A systematic review for structure optimization and clamping load design of large proton exchange membrane fuel cell stack.* Nov. 2020. DOI: 10.1016/j.jpowsour.2020.228724.

[9] Ke Song et al. *Assembly techniques for proton exchange membrane fuel cell stack: A literature review.* Jan. 2022. DOI: 10.1016/j.rser.2021.111777.

[10] J. G. Pharoah, K. Karan, and W. Sun. "On effective transport coefficients in PEM fuel cell electrodes: Anisotropy of the porous transport layers". In: *Journal of Power Sources* 161.1 (Oct. 2006), pp. 214–224. ISSN: 03787753. DOI: 10.1016/J.JPOWSOUR.2006.03.093.

[11] *EU considers ban on 'forever chemicals', urges search for alternatives | Reuters.* URL: https://www.reuters.com/markets/commodities/eu-considers-ban-forever-chemicals-urges-search-alternatives-2023-02-07/.

[12] N Bevilacqua et al. "Phosphoric Acid Invasion in High Temperature PEM Fuel Cell Gas Diffusion Layers". In: (2017). DOI: 10.1016/j.electacta.2017.10.054. URL: https://doi.org/10.1016/j.electacta.2017.10.054.

[13] Diankai Qiu et al. "Study on shape error effect of metallic bipolar plate on the GDL contact pressure distribution in proton exchange membrane fuel cell". In: *International Journal of Hydrogen Energy* 38.16 (May 2013), pp. 6762–6772. ISSN: 03603199. DOI: 10.1016/J.IJHYDENE.2013.03.105.

[14] Adnan Ozden et al. "A review of gas diffusion layers for proton exchange membrane fuel cells-With a focus on characteristics, characterization techniques, materials and designs". In: *Progress in Energy and Combustion Science* 74 (2019), pp. 50–102. DOI: 10.1016/j.pecs.2019.05.002. URL: https://doi.org/10.1016/j.pecs.2019.05.002.

[15] Xinting Wang, Ying Song, and Bi Zhang. "Experimental study on clamping pressure distribution in PEM fuel cells". In: *Journal of Power Sources* 179.1 (Apr. 2008), pp. 305–309. ISSN: 03787753. DOI: 10.1016/J.JPOWSOUR.2007.12.055.

[16] Zhiming Zhang, Jun Zhang, and Tong Zhang. "Endplate Design and Topology Optimization of Fuel Cell Stack Clamped with Bolts". In: *Sustainability (Switzerland)* 14.8 (Apr. 2022). ISSN: 20711050. DOI: 10.3390/su14084730.

[17] *Prescale - Pressure measurement film | Fujifilm [United States]*. URL: https://www.fujifilm.com/us/en/business/industrial-materials/measurement-film/prescale.

[18] E. Alizadeh et al. "Investigation of contact pressure distribution over the active area of PEM fuel cell stack". In: *International Journal of Hydrogen Energy* 41.4 (Jan. 2016), pp. 3062–3071. ISSN: 03603199. DOI: 10.1016/j.ijhydene.2015.12.057.

[19] Jiatang Wang, Jinliang Yuan, and Bengt Sundén. "On electric resistance effects of non-homogeneous GDL deformation in a PEM fuel cell". In: *International Journal of Hydrogen Energy* 42.47 (Nov. 2017), pp. 28537–28548. ISSN: 03603199. DOI: 10.1016/J.IJHYDENE.2017.09.119.

[20] Minkook Kim et al. "Bipolar plates made of plain weave carbon/epoxy composite for proton exchange membrane fuel cell". In: *International Journal of Hydrogen Energy* 37.5 (Mar. 2012), pp. 4300–4308. ISSN: 03603199. DOI: 10.1016/j.ijhydene.2011.11.125.

[21] Peng Liang et al. "Structure failure of the sealing in the assembly process for proton exchange membrane fuel cells". In: *International Journal of Hydrogen Energy* 42.15 (Apr. 2017), pp. 10217–10227. ISSN: 03603199. DOI: 10.1016/j.ijhydene.2017.01.026.

[22] Jinzhu Tan et al. "Chemical and mechanical stability of a Silicone gasket material exposed to PEM fuel cell environment". In: *International Journal of Hydrogen Energy*. Vol. 36. 2. Jan. 2011, pp. 1846–1852. DOI: 10.1016/j.ijhydene.2009.12.048.

[23] *What is Von Mises Stress in FEA? | SimWiki | SimScale*. URL: https://www.simscale.com/docs/simwiki/fea-finite-element-analysis/what-is-von-mises-stress/.

[24] *200723-hyperelastic*. URL: https://play.vidyard.com/BAyH7vvHptrcv7dQoG4myC.

[25] *Mooney-Rivlin hyperelastic model for nonlinear finite element analysis | by WELSIM - Engineering Simulation Software | Medium*. URL: https://getwelsim.medium.com/mooney-rivlin-hyperelastic-model-for-nonlinear-finite-element-analysis-b0a9a0459e98.

[26] *Newton-Raphson Method - an overview | ScienceDirect Topics*. URL: https://www.sciencedirect.com/topics/mathematics/newton-raphson-method.

[27] Christoph Roser. *"Faster, better, cheaper" in the history of manufacturing : from the Stone Age to lean manufacturing and beyond*, p. 411. ISBN: 9781498756303.

[28] *Hooke's law*. URL: http://labman.phys.utk.edu/phys221core/modules/m3/Hooke%27s%20law.html.

[29] "... within Epsilon Twin Cities ANSYS ® User Meeting Nonlinear Adaptivity". In: (2018).

[30] *ANSYS Mechanical – Overcoming Convergence Difficulties with Automatic Remeshing (Nonlinear Adaptive Region) - PADT*. URL: https://www.padtinc.com/2019/08/19/ansys-mechanical-overcoming-convergence-difficulties-with-automatic-remeshing-nonlinear-adaptive-region/.

[31] P. Lin, P. Zhou, and C. W. Wu. “A high efficient assembly technique for large PEMFC stacks. Part I. Theory”. In: *Journal of Power Sources* 194.1 (Oct. 2009), pp. 381–390. ISSN: 03787753. DOI: 10.1016/j.jpowsour.2009.04.068.